1988

Ultrastructural Studies of Cell Membrane-Associated Events in Early and Late Stages of Bovine Coronavirus Replication.

Harold Ross Payne
Louisiana State University and Agricultural & Mechanical College

INFORMATION TO USERS

The most advanced technology has been used to photograph and reproduce this manuscript from the microfilm master. UMI films the original text directly from the copy submitted. Thus, some dissertation copies are in typewriter face, while others may be from a computer printer.

In the unlikely event that the author did not send UMI a complete manuscript and there are missing pages, these will be noted. Also, if unauthorized copyrighted material had to be removed, a note will indicate the deletion.

Oversize materials (e.g., maps, drawings, charts) are reproduced by sectioning the original, beginning at the upper left-hand corner and continuing from left to right in equal sections with small overlaps. Each oversize page is available as one exposure on a standard 35 mm slide or as a 17″ × 23″ black and white photographic print for an additional charge.

Photographs included in the original manuscript have been reproduced xerographically in this copy. 35 mm slides or 6″ × 9″ black and white photographic prints are available for any photographs or illustrations appearing in this copy for an additional charge. Contact UMI directly to order.

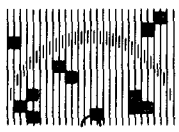

Accessing the World's Information since 1938

300 North Zeeb Road, Ann Arbor, MI 48106-1346 USA

Order Number 8819970

Ultrastructural studies of cell membrane-associated events in early and late stages of bovine coronavirus replication

Payne, Harold Ross, Ph.D.

The Louisiana State University and Agricultural and Mechanical Col., 1988

U·M·I

300 N. Zeeb Rd.
Ann Arbor, MI 48106

PLEASE NOTE:

In all cases this material has been filmed in the best possible way from the available copy. Problems encountered with this document have been identified here with a check mark __✓__.

1. Glossy photographs or pages ✓
2. Colored illustrations, paper or print
3. Photographs with dark background ✓
4. Illustrations are poor copy
5. Pages with black marks, not original copy
6. Print shows through as there is text on both sides of page
7. Indistinct, broken or small print on several pages
8. Print exceeds margin requirements
9. Tightly bound copy with print lost in spine
10. Computer printout pages with indistinct print
11. Page(s) _____ lacking when material received, and not available from school or author.
12. Page(s) _____ seem to be missing in numbering only as text follows.
13. Two pages numbered _____. Text follows.
14. Curling and wrinkled pages
15. Dissertation contains pages with print at a slant, filmed as received
16. Other

ULTRASTRUCTURAL STUDIES OF CELL MEMBRANE-ASSOCIATED EVENTS IN EARLY AND LATE STAGES OF BOVINE CORONAVIRUS REPLICATION

A Dissertation

Submitted to the Graduate Faculty of the
Louisiana State University and
Agricultural and Mechanical College
in partial fulfillment of the
requirements for the degree of
Doctor of Philosophy

in the

Veterinary Microbiology and Parasitology Option of

The Interdepartmental Program in

Veterinary Medical Sciences

by
Harold Ross Payne
B. S., University of Oklahoma, 1975
M. S., Louisiana State University, 1982
May 1988

ACKNOWLEDGEMENTS

These investigations were funded by United States Department of Agriculture Special Research Grants No. 80-CRSR-2-0650 and No. 86-CRSR-2-2871.

I wish to thank Drs. Johannes Storz and William G. Henk for their guidance and support throughout my doctoral studies. The other members of my graduate committee, Drs. M.D. Socolofsky, Kenneth Schnorr, Charles Issel, and William Todd are acknowledged for their valuable advice during my varied explorations.

I especially appreciate the contributions of my wife, Dr. Susan L. Payne, who provided me with intellectual stimulation and constant encouragement.

TABLE OF CONTENTS

LIST OF TABLES

LIST OF FIGURES

LIST OF ABBREVIATIONS

BCV	bovine coronavirus
BFS	bovine fetal spleen
CCV	canine coronavirus
DMEM	Dulbecco modified minimum essential medium
E	peplomeric protein
FFWO	fusion from without
FFWI	fusion from within
FIPV	feline infectious peritonitis virus
gp	glycoprotein
HCV	human coronavirus
HEV	hemagglutinating encephalomyelitis virus
HEPES	N-2-hydroxyethylpiperazine-N'-2-ethanesulfonic acid
HRT	human rectal tumor
IBV	avian infectious bronchitis virus
IgG	immunoglobulin fraction G
M	matrix protein
MEM	minimal Eagle's medium
MES	2-(N-morpholino)ethanesulfonic acid
MHV	murine hepatitis virus
MOI	multiplicity of infection
MW	molecular weight
N	nucleocapsid protein
N-linked	attached via ASN or LYS residue

O-linked	attached via SER residue
PBS	phosphate buffered saline
PEDV	porcine epidemic diarrhea virus
PFU	plaque forming unit
RCV	rat coronavirus
S	peplomeric protein
TCV	turkey coronavirus
TGEV	transmissible gastroenteritis virus
ts	temperature sensitive
um	micrometer

ABSTRACT

ULTRASTRUCTURAL STUDIES OF CELL MEMBRANE-ASSOCIATED EVENTS IN EARLY AND LATE STAGES OF BOVINE CORONAVIRUS REPLICATION

The early events in the infection of human rectal tumor cells by bovine coronavirus were investigated by immunoelectron microscopy and by studies with lysosomotropic weak bases. Virus particles labeled with colloidal gold were endocytosed by synchronously infected cells and accumulated in vacuoles that resembled secondary lysosomes. Sites of fusion between the virus envelope and the plasmalemma were observed but fusion events along intracellular membranes were not found. Exposure of cells to ammonium chloride or to methylamine during the first hour of infection had little inhibitory effect on the production of infectious virus. Chloroquine treatments were inhibitory but this effect was found to result from relatively late events in the infectious process. These studies indicate that an acidic intracellular compartment is not required for infectious entry by bovine coronavirus. Bovine coronavirus appears to penetrate the host cell barrier by direct fusion with the plasmalemma. Consistent with this interpretation, analyses of the culture environment conducive to virus-induced cell fusion revealed that the coronaviral fusion factor was active at alkaline pH levels.

Viral components were responsible for the induction of

cell-to-cell fusion. Immunoelectron microscopy was used to demonstrate that viral antigens were expressed in the plasma membrane of infected cells despite the intracellular mode for assembly of this virus. Cytopathic expression of the virus in cell monolayers produced turbid plaques. Scanning electron microscopy was used to characterize cells that remained in these plaques after the lysis of cells susceptible to the virus.

CHAPTER I: INTRODUCTION

Infection by bovine coronavirus (BCV) is a primary viral cause of neonatal bovine diarrhea. Substantial weight losses and mortality as high as 24% among newborn calves account for the economic impact of this syndrome (54).

BCV is a member of the Coronaviridae, a monogeneric family of large enveloped RNA viruses. Coronaviruses were first defined as a separate group in 1968 largely on the basis of shared virion morphology and antigenic relationships (150). Later studies have shown that coronaviruses also are distinguished by a unique transcriptional strategy (127), an exclusively intracellular viral morphogenesis (125), and by envelope glycoproteins with novel features (137).

Although the BCV strain originally described by Mebus (95) has been adapted to replicate in various cell cultures, the host cell range of other BCV strains is quite restricted. Many of these strains can be propagated in the adenocarcinoma-derived cell line HRT-18 (145). This line shares a variety of morphological characteristics with absorptive intestinal epithelial cells, the natural host cells of BCV in enteric infections (33, 34). HRT-18 cells and other lines have been used previously in morphological studies of BCV replicaton (144) but important aspects of the multiplication process remain unclear.

In the present investigations our aim was to analyze morphogenetic aspects of the membrane-associated events of BCV replication in cultured cells. The investigations addressed four specific objectives:

1. study and characterize the cellular processes and viral functions involved in BCV uptake
2. demonstrate and localize virus-specific antigens on the plasma membrane of cells infected with BCV
3. analyze the conditions required for BCV-induced polykaryocytosis in BFS cells
4. study the morphologic characteristics of BCV-induced plaques in HRT-18 cell monolayers.

Following a review of the pertinent literature, the succeeding chapters of this dissertation will describe the experiments conducted to realize the specific objectives. Each chapter is organized as a self-contained report for submission to a scientific journal. The manuscripts and journal to which they were submitted are as follows:

1. "Immunogold analysis of the early events in bovine coronavirus infection of cultured cells." Submitted to Journal of Virology. Co-authored by J. Storz and W.G. Henk.
2. "Bovine coronavirus antigens localized in the plasmalemma of infected cells". For submission to Journal of General Virology. Co-authored by J. Storz and W.G. Henk.
3. "Analysis of cell fusion induced by bovine coronavirus". For submission to Archives of Virology. Co-authored by J. Storz.
4. "Scanning electron microscopic characterization of bovine coronavirus plaques". For submission to Virus Research. Co-authored by W.G. Henk and J. Storz.

CHAPTER II: REVIEW OF THE PERTINENT LITERATURE

II.A. COMPARATIVE PROPERTIES OF CORONAVIRUS STRUCTURE.

Eleven coronaviruses were recognized as members of the family Coronaviridae in the Third Report of the Coronavirus Study Group of the Vertebrate Virus Subcommittee, the International Committee on Taxonomy of Viruses (124). These agents were identified as avian infectious bronchitis virus (IBV), human coronavirus (HCV), murine hepatitis virus (MHV), bovine coronavirus (BCV), transmissible gastroenteritis virus (TGEV), hemagglutinating encephalomyelitis virus (HEV), canine coronavirus (CCV), feline infectious peritonitis virus (FIPV), rat coronavirus (RCV), turkey coronavirus (TCV), and porcine epidemic diarrhea virus (PEDV).

II.A.1. Virion morphology. The distinctive virion morphology of the coronaviruses was originally a primary taxonomic characteristic of the group and is still used widely for tentative identification (50). In negatively stained preparations examined with the transmission electron microscope, coronaviruses appear as moderately pleomorphic particles 60-220 nm in diameter. Widely spaced, club-shaped peplomers project about 20 nm from the particle surface and produce the "corona" appearance for which the virus is named (125).

The peplomers of IBV are composed of two or three copies each of a pair of high molecular weight glycoproteins (17). MHV peplomers also consist of a pair of high molecular weight glycoproteins although the number of proteins per peplomer structure has not been determined (136). Among the coronaviruses, there are clearly discerned

morphological differences in the peplomers (26, 45). Furthermore, the virions of HEV (45), BCV (10), and MHV strain DIVIM (140, 141) reportedly have two different types of surface projections. The two peplomer types of BCV virions appear to be functionally distinct. King et al. (63) used bromelain to digest the large bulbous peplomers from BCV virions. This treatment left a short fringe of projections around particles and enhanced their hemagglutinating activity. Trypsin treatment produces BCV virions with shorter peplomers (135). This preparation appears to enhance viral infectivity (130).

Internal components of the virion typically are not apparent in negatively stained preparations. Bingham and Almeida (7), however, found tongue- or flask-shaped structures within IBV virions that were fixed in formaldehyde or treated very briefly with the detergent NP40. The internal component was apparently contiguous with the outer envelope. From the data, these workers proposed a morphological model for IBV which was supported by later studies of Lamontague et al. (77) who also extended the model to include BCV, HEV, and TGEV.

Internal structures have been described more frequently in thin sectioned coronavirions (125). Some investigators have described the coronaviral particles as two concentric membranes spaced by a clear zone that encircle a central core of variable density (25, 105). The inner shell may correspond to the flask-shaped internal component of Bingham and Almeida (7). Others have described internal doughnut-shaped or tubular strands in virions (50, 60). These images were interpreted as representing the viral nucleocapsid. In some

instances, electron microscopy of budding virions in thin sections suggests that the nucleocapsid symmetry is helical (91).

Purified coronavirions may be disrupted with nonionic detergents to release ribonucleoprotein cores or subviral particles. These structures were isolated after detergent treatment in the cases of coronaviruses TGEV (42), HEV (108), MHV (139), and HCV 229E (14, 60). Nucleocapsid structures may be isolated in density gradients at a higher density than intact virions. In sucrose, virions band at 1.18 g/ml whereas nucleocapsids band at approximately 1.27 to 1.28 g/ml (125). These nucleocapsid structures have been found to contain large amounts of the nucleocapsid protein of 50-60K and small amounts of the small envelope glyprotein, E1 (136). Sturman and coworkers (139) presented evidence that E1 is an RNA-binding protein. Electron microscopy of the subviral particles reveals nucleocapsids as spherical cores, 60-70 nm in diameter (42), sometimes containing a 9 nm in diameter strand (60). Negative staining of spontaneously disrupted virions occasionally has revealed helical, stranded, or tubular internal components (14, 81). Evidence for the structural organization of the nucleocapsid is equivocal because the conformation of this element appears to be susceptible to considerable distortion.

II.A.2. Genome stucture and organization. The viral genome is a large, continuous single-stranded RNA molecule that is 16 to 21 kilobases long (50). The genomic RNA of IBV has a 5′ cap structure, a 3′ polyadenylate tail, and is infectious (74, 80, 120). The

coronaviral genome contains no significant reiteration of oligonucleotides (125).

Coronavirus genomes have been compared by T1 oligonucleotide analyses in several studies (136). The investigations detected considerable differences between strains of MHV and also among isolates of IBV. The T1 oligonucleotide finger prints suggest that the coronaviruses have high rates of spontaneous mutation and that the RNA genome is quite variable.

The genetic organization of coronaviruses MHV (128, 157), TGEV (58), IBV (8, 9), and FIPV (27) have been the most closely studied. In each case, the 5′ gene, presumably the polymerase, is followed in sequence by structural genes for the peplomeric protein, the matrix protein and the nucleocapsid protein. Nonstructural genes were mapped at positions which differ among the viruses. A "leader sequence" located at the 5′ end of the genome is fused to each of the downstream genes to facilitate a unique mechanism of discontinuous transcription (127).

II.A.3. Structural proteins. Studies of coronaviral structural proteins revealed a complex diversity among mammalian and especially avian coronaviruses (125). The reported number of major components has ranged from as few as 3 to as many as 16 polypeptides in various studies. This variation resulted, in part, from actual differences between the gene products among coronaviruses (49, 63, 130) and from deviations in components of cleavage functions which are affected by both cellular and viral factors (41). Technical difficulties involving

contamination with host cell components (136) and artifacts induced by purification procedures (21) have contributed to the appearance of diversity as well.

As these factors were resolved, a pattern of 3 major protein structural elements was described for MHV-A59 by Sturman and coworkers (136). A similar pattern of 3 classes of proteins is generally applicable to most other coronaviruses (16, 17, 62, 82). Differences remain in the exact number of proteins, their molecular weights, and their interrelationships. The major classes of proteins are identified as: the peplomer protein(s), S or E2; the nucleocapsid protein, N; and the matrix protein(s), M.

The large surface peplomers of the virion are formed by one or two species of high molecular weight glycoproteins. Cavanagh (17) reported that the S protein of IBV is a oligomer with an apparent molecular weight of about 354,000 which is composed of two glycopeptides, S1 (90K) and S2 (84K) in equimolar proportions. These proteins are noncovalently associated and only S2 is anchored to the virus envelope. The peplomeric glycoprotein of MHV (E2) is synthesized as a 180K precursor which undergoes maturational cleavage to form two subunits (90A and 90B) with identical electrophoretic mobilities (112, 136). The large bulbous peplomers of BCV are composed of a 190K glycoprotein which is normally present as subunits of 120K and 100K (221). BCV has an additional high molecular weight glycoprotein, gp140, which is absent from MHV-A59 (31, 63). This glycoprotein, a hemagglutinin, is a dimer of disulfide linked 65K subunits. Another hemagglutinating coronavirus, HEV, also has a high molecular weight

glycoprotein, gp130/74, in addition to its peplomeric glycoproteins (10).

The N protein is a nonglycosylated RNA binding protein with a molecular weight of 50-60K (125). This nucleocapsid protein is phosphorylated by a serine kinase that is virion associated (123). The identity of the kinase protein itself has not been determined and the function of N protein phosphorylation is obscure. Sturman et al. (139) found that the matrix protein, E1, of MHV binds specifically with the RNA component of the nucleocapsid rather than with the N protein.

The coronavirus M protein is an envelope glycoprotein of 20 to 30K molecular weight with 1 to 4 additional polypeptides of similar size (136). The additional polypeptides probably represent glycosylation isomers, at least in the cases of MHV (114), IBV (15), and BCV (31, 78). The M protein of MHV is largely buried in the viral envelope by three successive membrane spanning helices followed by a carboxy-terminal random coil embedded in the inner face of the virion membrane (118). The matrix proteins of MHV (103) and BCV (122) bear O-linked oligosacccharides whereas TGEV (86) and IBV (132) matrix proteins have only N-linked oligosaccharides.

II.A.4. Envelope properties. The lipid composition of the viral envelope roughly corresponds to the composition of the membranes of the cells in which it was propagated (68, 136). The envelope of TGEV contains less cholesterol and fatty acid than is present in the plasma membrane and therefore may more nearly reflect the composition of intracellular membranes where budding takes place (136).

Alternatively, the acyl side groups and hydrophobic intramembrane regions of the envelope proteins may selectively enrich or deplete membrane components before virus envelopment. Cell-derived glycosaminoglycans are associated with the external surfaces of the envelopes of TGEV (42) and MHV-A59 (139). Virion-associated glycosaminoglycans are potentially important in alterations of many viral functions.

II.B. ENTRY OF ENVELOPED VIRUSES INTO ANIMAL CELLS.

II.B.1. Cellular adsorption of virus. The initial step in virus entry is attachment of the virions to the host cells. This attachment involves recognition and binding of a cellular receptor by a viral attachment protein. In enveloped viruses, glycoproteins of the spikes or peplomers apparently fulfill this attachment function (68). MHV-A59 particles competed with purified peplomeric glycoprotein (E2) for viral receptors on the cell surface (136). Furthermore, monoclonal antibodies against the peplomeric proteins of MHV-JHM indicated that the 170K glycoprotein of this strain is the viral attachment protein (20). These studies demonstrate that the high molecular weight class of coronaviral glycoproteins mediates adsorption of the virus. Attachment of MHV-A59 to L cells occurs readily at $4^{0}C$ and more quickly at $37^{0}C$ (72). Patterson and Macnaughton (106) employed scanning electron microscopy to study the morphological characteristics of HCV adsorption to cultured cells. The coronavirions were initially attached over the whole cell surface but rapidly were redistributed away from the cell periphery by an energy dependent mechanism.

A related viral function, adsorption to erythrocytes, is responsible for the phenomena of hemagglutination and hemadsorption. Coronaviruses that agglutinate erythrocytes include some strains of BCV (121), HEV (46), IBV (22), HCV-OC34/43 (59), and MHV-3 (142). HEV adsorption to avian erythrocytes is mediated by binding sites at the tips of the peplomers (97). Cells infected with hemagglutinating enveloped viruses typically adsorb erythrocytes to the cell surfaces. It is unclear, in the case of BCV-infected cells, whether the erythrocytes adsorb to viral hemagglutinins in the plasma membrane (hemadsorption) or to accumulated virions at the cell surface (pseudohemadsorption) (94).

II.B.2. Envelope fusion and nucleocapsid release. The adsorbed virus must overcome membrane barriers during the entry process to accomplish nucleocapsid release and infection. Animal viruses effect nucleocapsid release by fusion of the viral envelope with a cell membrane (126). Membrane fusion is catalyzed by viral envelope proteins which function at pH optima that are characteristic of the particular virus (160). Two separate pathways, direct and endocytic, are recognized for the entry of animal viruses into host cells (79).

The direct pathway for entry involves fusion of the viral envelope with the plasma membrane. This route is taken by a limited number of viruses, primarily members of the paramyxovirus (38, 109) and herpesvirus (38) groups, with fusion proteins that are active at physiological pH.

The endocytic route appears to be a more commonly used route for virus entry. Studies have indicated that togaviruses (47, 48), bunyaviruses (43), retroviruses (3, 110), orthomyxoviruses (92) and rhabdoviruses (55) effect entry by this indirect route. A widely accepted model has been developed for virus entry by the endocytic pathway (88). According to the model, these viruses are unable to enter directly at the plasma membrane because their fusion proteins are fusogenic only in low pH conditions. The adsorbed virus particles, therefore, are internalized by adsorptive endocytosis, a cellular process for the uptake of receptor-bound nonphysiological ligands. In this process, the receptor-bound virus particles are collected in clathrin coated pits, sequestered in coated vesicles and delivered to prelysosomal structures known as endosomes. The coated vesicles and endosomes contain an electrogenic ATP-dependent proton pump (40) that creates the acidic conditions found in the vacuole lumen (149). The acidic environment induces viral envelope fusion with the vesicle membrane, and the virus nucleocapsid is released into the cytoplasmic sap.

This model is based primarily on two apparently related observations. First, experiments with lysosomotropic weak bases indicate that infection by the endocytic pathway involves virus passage through an acidic cellular compartment. The bases which include chloroquine, amantadine, ammonium chloride, and methylamine accumulate in acidic compartments of the cell and increase the pH level of those compartments (93, 104). This treatment inhibits an early stage of virus replication and greatly reduces virus production (47, 48).

Viruses susceptible to this type of inhibition are those unable to enter the cell by direct fusion (47).

Secondly, it was observed that brief exposure to low pH conditions can trigger induction of cell to cell fusion by many viruses. Semliki forest virus (48, 158) and fowl plague virus (92) trigger cell fusion only at low pH, and they require an acidic compartment for entry as well. In fact, Helenius et al. (158) found that a chloroquine-imposed block on Semliki forest virus infectious entry can be overcome by inducing virus fusion at the plasma membrane with low pH treatments. Furthermore, mutants of Semliki forest virus were generated that display alterations in their sensitivity to lysosomotropic agents and corresponding differences in the pH threshold required for induction of cell to cell fusion (61). These findings, which are incorporated in the model, indicate that the requirement for an acidic compartment for virus entry is related to the possession of pH dependent fusion proteins.

II.B.3. Genome uncoating. Uncoating involves the topological removal of envelopes and capsids to enable the viral nucleic acids to interact with ribosomes or polymerases. The last step in uncoating is the dissociation of protein from the nucleic acid. Specific information about uncoating of the coronavirus genome has not been reported. On the basis of the data available on other positive-strand RNA viruses, Wilson (162) suggested that nucleocapsid disassembly is a cotranslational "event". According to this hypothesis, the following steps are involved. Viral nucleocapsids arrive more or less intact

within the cytoplasm of infected cells but with some structural changes. The encapsidated RNA is therefore at least partially protected from attack by ubiquitous cellular RNAses. Ribosome binding to an exposed 5′ leader sequence and subsequent translocation lead to sequential disassembly of the nucleocapsid. The early gene product, RNA-dependent RNA polymerase may then bind to the 3′ end of the genome and, possibly, initiate disassembly in the 3′ to 5′ direction.

II.B.4. Modes of coronavirus entry. Few detailed studies of coronavirus entry and uncoating have been performed. Although electron microscopic studies generally have indicated that coronaviral entry is by means of endocytosis (25, 72, 107), other investigators have suggested that coronaviruses enter the cell by fusion with the cell membrane (18, 34). Krzystyniak and Dupuy (72) presented kinetic data indicating that MHV-3 uptake by macrophages is time- and temperature-dependent and that the process is insensitive to inhibitors of phagocytosis.

The effects of lysosomotropic agents on murine coronaviruses have been examined in several studies. Malluci (86) reported in 1966 that macrophages treated for long periods with chloroquine before MHV infection produce markedly less virus than untreated cells. More recenty, the effects of ammonium chloride and chloroquine on MHV-3 infection of L cells was examined (73). At very low multiplicities of infection, MHV production at 18 to 24 h post infection was inhibited by these agents. Mizzen and coworkers (98), examined more closely the effects of ammonium chloride on MHV entry. Their work indicated that

the drug suppresses the ultimate number of cells infected by attenuating the uncoating process rather than by imposing an absolute block on infection. Although most of the evidence available supports an endocytic route of entry for murine coronaviruses, details of the uptake mechanism are unclear. This statement is particularly true for coronaviruses such BCV which have poorly characterized membrane fusion proteins.

In addition, recent investigations (153) have revealed that host cell characteristics can play a decisive role in the success of virus entry. These investigators described a defective entry process in rat glial C6 cells that renders them resistant to infection by MHV-JHM and MHV-A59. This defect apparently involves a restricted entry mechanism because virus introduced into the cells by polyethylene glycol fusion replicates successfully and is released. Subsequent spread of the progeny virus in the C6 monolayer is inhibited by fusion resistance.

II.C. SUBSEQUENT EVENTS IN CORONAVIRUS REPLICATION.

II.C.1. Events in primary translation. RNA-dependent RNA polymerase is not found as part of the coronavirion but enzyme activity can be detected in coronavirus-infected cells (30, 83). Presumably, the incoming coronavirus genome serves as messenger RNA for the synthesis of the RNA-dependent RNA polymerase. The protein products of this primary translation are not detected in infected cells prior to transcription. Cell-free translation of virion RNA results in the synthesis of two putative polymerase gene products (29), one of which was identified in infected cells labeled at late times after infection.

II.C.2. Synthesis of mRNAs and progeny genomes. The RNA-dependent RNA polymerase transcribes the viral genome into a full-length negative strand RNA (76). This species serves as the template for synthesis of genomic-sized mRNA and a group of 5 or 6 subgenomic mRNAs, depending upon the particular coronavirus (27, 58, 127, 128). Oligonucleotide mapping revealed that the mRNA structures form a nested set with 3′ coterminal ends extending different lengths in the 5′ direction (133). Coronavirus subgenomic mRNAs are generated by a fusion of non-contiguous nucleic acid sequences during mRNA synthesis (75, 127). A "leader sequence" is transcribed from the 3′ end of the negative strand RNA and the nascent RNA often dissociates from the template. Free leader RNA can rebind to the template at the initiation sites of the various mRNAs and serve as a primer for continued transcription (85). A recent analysis revealed a temporal regulation for the differential synthesis of subgenomic mRNAs and genomic RNA in cells infected with BCV (59a). The frequency of transcription of each mRNA species appears to be regulated by the number of homologous nucleotides at the intergenic binding site (75).

II.C.3. Protein synthesis and posttranslation modifications. Only the "unique" 5′ proximal gene of each mRNA is translated. Coronavirus mRNAs apparently are functionally monocistronic and most do not direct the synthesis of polyprotein precursors, in contrast to other positive-strand RNA viruses. The nucleocapsid protein and the nonstructural proteins are synthesized on free ribosomes (122,134).

The N protein of MHV-JHM is synthesized as a protein with a molecular weight of approximately 57,000 (134). This precursor, found exclusively in the cytosol, is phosphorylated immediately after synthesis by a serine kinase (120) and associates with the membrane fraction as a phosphoprotein with an apparent molecular weight of 60K (125).

The mRNA encoding the peplomeric protein (S or E2) is translated on ribosomes bound to membranes of the endoplasmic reticulum. Precursors of the IBV peplomeric protein possess an N-terminal 18 amino acid sequence, presumably a membrane insertion signal sequence, that is absent from the mature glycoprotein (8). Oligosaccharide side chains of the peplomeric glycoproteins are attached by acetylglucosamine linkages to asparagine residues of the polypeptide (111, 115). Biosynthesis of asparagine-linked (N-linked) oligosaccharides involves assembly of a precursor form of the oligosaccharide onto a dolichol phosphate lipid intermediate, in a process sensitive to the antibiotic tunicamycin (164). The preassembled structure is transferred en bloc from the dolichol molecule to the nascent polypeptide in the cisternal space of the rough endoplasmic reticulum. The high mannose N-linked oligosaccharides subsequently are converted in the Golgi apparatus to complex type oligosaccharides in a sequence of steps involving the trimming of mannose residues and the addition of other sugars (143). MHV E2 is acylated by the covalent addition of palmitic acid (111, 132). Proteolytic cleavage of MHV E2, either by cellular proteases acting on E2 during virus maturation or by the addition of a protease to released

virions, is required to activate MHV-induced cell fusion (50). The fusion of BCV-infected cells also is enhanced by the presence of trypsin (135).

The matrix protein, also sythesized on membrane bound ribosomes, differs substantially from E2 in its insertion and processing. Although a cellular signal recognition particle for membrane insertion is required (117), the matrix proteins of MHV and IBV possess internal rather than of N-terminal signal sequences (116, 117, 118). In contrast to their peplomeric glycoproteins, the matrix proteins of MHV (115) and BCV (53) are glycosylated posttranslationally and bear only O-linked oligosaccharides. These structures were the earliest discovered viral envelope proteins with O-linked oligosaccharides. The O-linked glycosylation process is insensitive to tunicamycin treatment. The matrix proteins of TGEV (58) and IBV (132), however, bear N-linked oligosaccharides.

II.C.4. Role of cellular organelles in coronavirus assembly and maturation. Coronaviruses assemble by budding at intracellular membranes, presumably at sites defined by the matrix glycoprotein (35, 91). Assembly involves an interaction at the cytoplasmic face of the membrane between the viral nucleocapsid and the carboxy terminal portion of the matrix glycoprotein (118, 139). The intracellular location of the matrix glycoprotein is restricted to internal membranes of the cell by an undetermined targeting mechanism (53, 116). Initial budding of coronaviruses usually occurs at membranes of the Golgi and smooth endoplasmic reticulum (2, 16, 25, 34, 70) but host cell factors

rather than viral functions determine the intracellular compartments into which MHV buds. For example, the budding of progeny MHV virions in AtR20 cells is restricted to the Golgi cisternae (4), whereas the rough endoplasmic reticulum is a major site of assembly of progeny MHV virions in sac(-) cells (147). In the latter case, the virus particles are transported through the Golgi apparatus where the envelope proteins undergo O-linked glycosylation and final trimming of N-linked oligosaccharides. The rough endoplasmic reticulum and the Golgi vesicles typically become dilated with accumulated virus particles and electron-dense granulo-fibrillar material (25, 33, 34, 36).

Investigations of the effects of monensin treatment suggest that the Golgi apparatus is also involved in the release of progeny coronavirus from intact cells. Monensin is a sodium ionophore that blocks glycoprotein transport to plasma membranes at the level of the Golgi (143). Nieman and coworkers (102) found that monensin treatment of MHV-infected cells prevents O-linked glycosylation of the M protein. Budding of MHV continued in the presence of the ionophore, but release of the assembled particles was inhibited. The role of lysosomes in coronavirus infection was examined by Ducatelle and Hoorens (36). They reported that accumulated coronavirus particles often can be found in secondary lysomes at late stages of the infection. Although lysosomal enzymes seemed unable to destroy the accumulated viruses, it was suggested that these structures represent an intracellular defense mechanism.

II.D. INDUCTION OF CELL FUSION BY ENVELOPED VIRUSES.

II.D.1. Significance of cell fusion for cytopathogenesis. The infectivity of an enveloped virus is modulated by its fusion activity which is required both for the initial infection and for transmission of progeny virus to neighboring cells. The outcome of coronavirus infections can be determined by the ability of the host cell to activate the viral fusion factor (41). This observation may be responsible, in part, for the stringent requirements of many newly isolated coronaviruses for differentiated cells. Resistance to membrane fusion by a particular host cell type can minimize polykaryon formation and reduce virus spread (99). Fusing properties are overtly expressed by a variety of enveloped viruses (69). Induction of polykaryon formation is a cytopathic effect often signaling approaching cell death (68). For example, cell fusion is a major factor in early cell death caused by measles virus (44). Fusion activity is probably a virulence factor in vivo. Multinucleated cells are characteristic of many coronavirus-induced lesions.

II.D.2. Events of virus-induced cell fusion. Entry of an enveloped virus into its host cell involves a membrane fusion event that is catalyzed by viral fusion proteins. Virus fusion with the host cell plasma membrane may also occur in an amplified form resulting in the formation of polykaryons (160). Polykaryocytosis is thought to result from the action of viral fusion proteins on the plasma membranes of adjacent cells. Although this phenomenon has long been described,

the actual molecular events occurring during the fusion process are still controversial. Virus-induced polykaryon formation may proceed by either fusion from without (FFWO) or fusion from within (FFWI) (68). FFWO occurs soon after infection when massive numbers of the enveloped viruses fuse simultaneously with the plasma membrane of the cells. FFWI, an event occuring late in the infection, is catalyzed by fusion proteins that are expressed at the plasma membrane of infected cells (160). Virus-induced cell fusion and the fusion event of virus entry have different effects on cellular integrity. Entry by fusion is innocuous in itself but cell death ultimately results from the massive assault of virus-induced cell fusion (68).

II.D.3. pH dependence of virus-induced cell fusion. Fusion activity of enveloped viruses is routinely studied indirectly by assays of virus-induced cell fusion. Cell fusion can be induced at physiological pH by paramyxoviruses (55) and some strains of herpes simplex virus (38). The pH-independent fusion activity of these viruses will induce FFWO of appropriate target cells that are infected at high multiplicity. FFWI occurs spontaneously among paramyxovirus-infected cultured cells following expression of viral fusion proteins in the plasma membrane (160).

Many other viruses, including togaviruses (47, 158, 159), influenza viruses (57, 92, 159), rhabdoviruses (110), retroviruses (110), and bunyaviruses (43), have been found capable of inducing fusion of cultured cells but only at nonphysiological pH. Induction of FFWO by these viruses requires that high multiplicities of virus be

adsorbed to the cell surface. The virus-cell complex is then briefly exposed to acid pH and returned to neutral pH to allow fusion to proceed (160). The pH-dependent fusion activity of such viruses can also be demonstrated by FFWI triggered by acidic conditions (43, 61, 110). For this purpose, virus-infected cell monololayers are exposed briefly to acidic medium then incubated at physiological pH to allow fusion to proceed. The minimum pH level required to induce pH-dependent fusion is characteristic of the particular virus.

Studies of pH-dependent viral fusion indicate that polykaryon formation ensues when acidification activates viral fusion proteins that are positioned at the plasma membrane (160). The required acidic conditions are hypothesized to mimic the conditions within endosomes where the fusion event of virus entry takes place. Virus-induced pH-dependent cell fusion appears to be a two step process, however. Investigations have found that although acidic conditions are required to induce fusion of cultured cells, membrane fusion itself occurs only after the pH is returned to neutral conditions (37, 87). There is no evidence that the pH of the endosome fluctuates from acid to neutral pH.

II.E. PERSISTENCE OF CORONAVIRAL INFECTIONS.

II.E.1. Chronic demyelinating disease in rodents. Many coronaviruses appear to be capable of inducing chronic infections in animals (125). Chronic demyelination in the rodent central nervous system is an important part of the disease spectrum that may be produced by MHV infection (67). Hosts of the appropriate age and

genetic background inoculated intracerebrally with high doses of wild type MHV develop an acute lethal disease (65, 155). A chronic demyelinating disease in mice is produced by low doses of wild-type virus or high doses of attenuated temperature-sensitive mutants of MHV-A59 or MHV-JHM (71, 154, 156). Koga (67) described the sequence of neuropathological events in chronic demyelinating disease. Initially, clinically silent lesions of acute encephalitis develop which do not enlarge following a rise in neutralizing antibodies. At this time, demyelinating lesions are found which are characterized by infection and lysis of oligodendrocytes with little damage to axons. Previous workers reported that mice with MHV-induced demyelination often recover with apparent remyelination but develop a persisting or recurring demyelination (49). Sorenson and Dales (126a) demonstrated that coronaviral RNA persists in Purkinje neurons of the cerebellum of rats that undergo prolonged infections. These cells may function as virus repositories and provide a reservoir of infectious virus throughout the prolonged asymptomatic phase of MHV-JHM infection.

Several factors in MHV-induced encephalomyelitis may prevent nonfatal infection and instead cause a nonlethal chronic demyelination disease. The emergence of viral mutants attenuated by altered cell tropism is implicated. A temperature-sensitive mutant of MHV-JHM, (ts-8) causes a high incidence of demyelination with low mortality (66). The mutant causes selective destruction of oligodendrocytes and preferentially destroys nonneuronal cells of the CNS <u>in vitro</u> (35). Koolen et al. (71), presented evidence suggesting that tissue tropism of another mutant, ts-342, determines restricted replication and

attenuated virulence of this variant. Replication of ts-342 was restricted to the brain in vivo and the agent induces subacute demyelinating disease. Revertants spread from the brain and cause fulminant hepatitis, the apparent cause of death of mice infected with wild-type virus (71). Virus-specific antibodies seem to play a role in the development of acute or chronic disease. Antibodies were found to block the infection of neurons but not oligodendrocytes (11). Also, mutations of the peplomeric protein confer resistance to neutralization by monoclonal antibodies and these virus variants induce a subacute demyelinating disease rather than an acute encephalomyelitis (24, 39).

II.E.2 Persistence of coronaviral infections of cattle. The enteric coronaviruses, which may cause severe diarrheal disease in newborn or infant animals, characteristically produce mild or inapparent persistent infections in adults (50). Collins et al. (20a) found that the incidence of shedding of enteric coronavirus from adult cattle increased from 20% to 30% during the last two months of gestation to 65% to 70% at parturition. Coronavirus shedding at parturition may result in immediate exposure of neonates at an age when they are highly susceptible to infection with the virus. The immune responses of clinically normal cows that chronically shed bovine coronavirus-specific immune complexes was studied by Crouch et al. (23). The infection was not cleared despite the presence of both fecal and serum antibody. Immunosuppression was experimentally induced by dexamethasone treatment. The drug temporarily reduced shedding of

virus-specific immune complexes but further analyses of this effect failed to establish any major role for cell mediated immunity in maintaining the chronic infection.

II.E.3. Mechanisms of coronaviral persistence in cultured cells. Persistent or inapparent infections can be described as those in which the virus infects and kills only a small percentage of cells in the culture (68). Coronaviruses, in contrast to other positive-stranded viruses, tend to establish persistent infections in cultured cells (125). Possible mechanisms involved in the establishment of persistent coronaviral infections include conditional interference by emerging temperature-sensitive or poorly growing mutants (71), the development of defective interfering virus (84), and the production of interferon (5). Baybutt et al. (6), described the production of a long-term persistent infection established in the murine cell line sac(-). A heterogenous collection of temperature-sensitive mutants was identified among the virus progeny. The investigators argued that the temperature-sensitive phenotype itself was probably insignificant in the establishment of the persistently infected culture and arose as an "effect" rather than a "cause" of persistence. These workers established that low multiplicity of infection favored the establishment of persistent infections. Interferon was apparently not involved in maintenance of persistence.

The generation of defective interfering particles by MHV-infected cultures was reported by Makino et al. (84). In the course of serial

undiluted passages of MHV-JHM virus in cell culture, they found markedly reduced infectivity. The progeny viruses interfered with the replication of the original wild type JHM virus, lacked part of the viral genome, and possessed other properties of defective interfering particles. Regulation of a persistent coronavirus infection by a host cell determinant was examined by Mizzen et al. (99). MHV-induced fusion was markedly reduced in LM-K cells as compared to L-2 cells. Their investigation indicated that the inherent resistance of the LM-K cell membrane moderates virus dissemination and contributes to the state of virus persistence.

CHAPTER III: EARLY EVENTS IN BOVINE CORONAVIRUS INFECTION OF CULTURED CELLS

III.A. INTRODUCTION.

Bovine coronavirus (BCV) is a member of the Coronaviridae family of enveloped RNA viruses (125). BCV replicates in absorptive epithelial cells of the intestinal tract in neonatal calves and induces serious enteric disease (54). Although many features of coronavirus replication in cultured cells have been described (25, 36, 70, 73, 97, 147), the early events of BCV infection remain poorly characterized.

At least two distinct pathways evidently operate for the entry of enveloped viruses into animal cells (79). Some viruses penetrate the cell by direct fusion of the viral envelope with the plasma membrane. Paramyxoviruses, for example, fuse directly with the cellular plasma membrane at physiological conditions (109). Other viruses fuse with membranes only under nonphysiological, low pH conditions (47, 109, 159). The second pathway for enveloped virus entry involves cellular uptake by endocytosis (88, 89, 90, 92). The endocytosed virions travel to membrane bound intracellular compartments where acidic conditions are maintained (40, 149). The low pH of this cellular compartment apparently facilitates fusion between the viral envelope and the vesicle membrane and results in release of the nucleocapsid into the cytoplasm. Infection of cultured cells by a variety of enveloped viruses can be blocked with lysosomotropic weak bases (3, 47, 92, 98). These bases accumulate in acidic cellular compartments and alter their pH (93). The change apparently prevents low pH-dependent viral

envelope fusion with the vesicle membrane and thus block infection (48).

Studies of inhibition by lysosomotropic agents indicate an endocytic mechanism for the entry of mouse coronavirus (73, 98, 146) but the validity of this experimental approach has recently been questioned (13). In order to establish the route of entry for BCV, we examined the early events of the infection process not only by infectivity and inhibition studies but by immunoelectron microscopy as well.

III.B. MATERIALS AND METHODS.

III.B.1. Cells and virus. Monolayers of the human rectal tumor cell line HRT-18 (145) were grown in Dulbecco modified Eagle medium (DMEM) containing streptomycin sulphate (0.1 mg per ml), penicillin (100 units per ml), and 5% fetal calf serum. The Mebus strain L9 of bovine coronavirus (121, 131) was propagated in HRT-18 cells. Virus stocks were prepared in cells infected at a multiplicity of approximately 0.01 PFU per cell, incubated for 4 to 5 days at 37^{0}C in serum-free DMEM and harvested by freeze-thawing. Viral titers obtained in these preparations ranged from 10^6 to 10^7 PFU per ml.

III.B.2. Plaque assays. The infectivity titer was assayed in HRT-18 monolayers grown in 6-well plates. The monolayers were adsorbed with virus for 1 h at 37^{0}C, overlayed with serum-free DMEM containing 0.6% agarose (Bethesda Research Laboratories) and 4 ug of trypsin

(Difco Laboratories) per ml. After 3 days of incubation at 37°C, plaques were counted without staining.

III.B.3. Virus purification and concentration. Infected cultures were harvested at 4 d post infection when more than 50% of the cells showed evidence of virus infection. The infected material was subjected to two freeze-thaw cycles and sonic disruption (Ulrasonic 250; Branson Sonic Power Company) for 30 sec on ice to release the virus. The virus suspension was clarified by centrifugation at 10,000 x g for 40 min, sedimented at 90,000 x g for 2 h through a 20% sucrose cushion, and resuspended in DMEM (pH 7.4) buffered with 12 mM HEPES and 25 mM $NaHCO_3$ (uptake medium). The recovery of infectious virus ranged from 50% to 75%.

III.B.4. Immunoreagents. Rabbit antiserum to BCV that had been purified from infected bovine fetal kidney cells was prepared by previous investigators in our lab. The antibody level was titered by a plaque neutralization test. The IgG fractions of the antiserum and of normal rabbit serum were obtained by protein A-sepharose column chromatography. Goat anti-rabbit antibody (IgG) complexed to 5-nm colloidal gold particles manufactured by Janssen Life Sciences Products, Beerse, Belgium was used. For virus internalization experiments, the immunoreagents were diluted in uptake medium to levels producing less than 50% neutralization of viral infectivity.

III.B.5. Immunogold labeling of virus entry. Cell monolayers, grown in 2-well chamber slides (Miles Scientific), were rinsed with uptake medium, chilled to 4°C, and reacted with purified virus for 60 min at a multiplicity of 50 PFU per cell. The virus-cell complexes were incubated on ice for 45 min with rabbit anti-BCV antibody, washed twice with uptake medium, and incubated for 45 min with gold-labeled goat anti-rabbit antibody. After washing at 4°C, the cells were rapidly warmed to 37°C and incubated for various lengths of time before primary fixation at 4°C with 2% glutaraldehyde and 2% formaldehyde in 0.1 M sodium cacodylate buffer at pH 7.4.

III.B.6. Processing for electron microscopy. The monolayers were then fixed for 1 h at 25°C in a solution of 1% osmium tetroxide and 1% potassium ferrocyanide in 0.1 M cacodylate buffer (pH 7.4), washed in 0.2 M sodium acetate buffer pH 3.5, and stained en bloc for 1 h with 0.2% uranyl acetate in acetate buffer. After washing in distilled water, the cells were dehydrated in an ascending alcohol gradient, embedded in situ in a mixture of Epon and Araldite epoxy resins (100), and polymerized at 60°C. Thin sections were stained with uranyl magnesium acetate followed by lead citrate and viewed with a Zeiss EM-10 electron microscope at 80 kV.

III.B.7. Effects of lysosomotropic agents. Monolayers of HRT-18 cells were grown in 24-well plates for experiments involving treatments with lysosomotropic agents. Infection of HRT-18 cells by BCV was synchronized by temperature shift to analyze the relative effects of

chloroquine, ammonium chloride, methylamine, and amantadine. Monolayers were washed with medium, chilled to 4°C, adsorbed for 60 min with BCV at a multiplicity of approximately 3 PFU per cell, and rinsed with cold uptake medium to remove unadsorbed virus. The monolayers were given warm medium with the appropriate lysosomotropic agents and transferred to a 37°C incubator. In control monolayers, exposure to the agent was delayed until 1 h post infection. All cultures were harvested after incubation for 20 h at 37°C, and the yield of infectious virus was titered by plaque assays.

The effects of various concentrations of ammonium chloride and chloroquine on virus infection at 37°C was tested on monolayers that were washed with uptake medium and pretreated for 15 min with the agent diluted in uptake medium. The cells were infected with BCV at 37°C for 60 min at a multiplicity of approximately 3 PFU per cell and then fed fresh uptake medium. The lysosomotropic agent was present throughout the infection. Exposure to the agent was delayed until 1 h post infection in control monolayers. After incubation for 20 h at 37°C, the cultures were harvested and the yield of infectious virus was titered by plaque assays.

The time dependence of inhibition by 120 uM chloroquine was analyzed by measuring the effects of increasing delays in chloroquine addition. The monolayers were synchronously infected as described above except that chloroquine was first added to the cultures at various times after rewarming. After incubation at 37°C for 20 h, the virus titer was determined by plaque assay.

The pH dependence of chloroquine inhibition was determined with monolayers that were allowed to bind BCV at 4^{0}C and then were washed with cold DMEM. The cells were warmed to 37^{0}C for 60 sec by the addition of DMEM buffered with 12 mM HEPES and 12 mM MES at various pH levels and given fresh uptake medium with 120 uM chloroquine. Chloroquine was added at 1 h post infection for a final concentration of 120 uM in all monolayers, and after a 20 h infection the virus titer in the culture was determined by plaque assay.

III.B.8. Indirect immunofluorescence. Monolayers were fixed for 10 min in 4% formaldehyde, permeabilized for 5 min with acetone at -20^{0}C, incubated with rabbit anti-BCV antibody, and reacted with goat anti-rabbit antibody conjugated to fluorescein isothiocyanate. The preparations were viewed with a Leitz fluorescent microscope using epifluorescence. The fraction of infected cells in each preparation was calculated from 5 randomly selected fields of approximately 200 cells photographed with both phase contrast and fluorescence optics.

III.B.9. Chemicals. Stock solutions were prepared daily of 20 mM chloroquine-HCl, 200 mM amantadine-HCl, 1.0 M ammonium chloride, and 4.0 M methylamine (Sigma Chemical Company) in saline. The solutions were adjusted to neutral pH with NaOH, and diluted into uptake medium.

III.C. RESULTS.

III.C.1. Morphologic analysis of BCV adsorption. Cells adsorbed with BCV particles and immunolabeled at 4^{0}C reveal that coated

pit formation had ceased leaving all virions at the cell exterior (FIG. III.1). The virions were readily identified by the associated colloidal gold particles. The use of highly dilute anti-BCV antibody labeled most virions with only a few gold particles. These particles were separated from the viral envelope by an average distance of about 15 nm. The virus particles usually contained an electron dense core and were spherical in shape with diameters ranging from 50 to 80 nm. Virions with ellipsoidal profiles also were observed. The viral envelope was separated from the plasma membrane by a distance of less than 15 nm in many cases. Fibrillar connections were evident at the plasma membrane attachment site (FIG. III.1A, inset) but the peplomer structures of BCV, distinctive in negative stains, could rarely be distinguished. The number of virus particles per cell appeared to exceed what would be expected from the input multiplicity (50 PFU per cell). This is probably because (i) the virus particles were adsorbed by only a small minority of HRT-18 cells in the monolayer and (ii) many of the virus particles were not infectious.

III.C.2. Endocytosis of BCV at 37^{0}C. Virus particles at intracellular locations were morphologically less readily distinguished. The associated gold label, however, permitted identification of the intracellular sites of virus particles during uptake. After the BCV-cell complexes were incubated for 2 to 5 min at 37^{0}C, labeled virus particles were evident in coated pits, coated vesicles and in small multiform vesicles with smooth membranes (FIG. III.2). Coated vesicles had circular profiles of 100 nm in diameter,

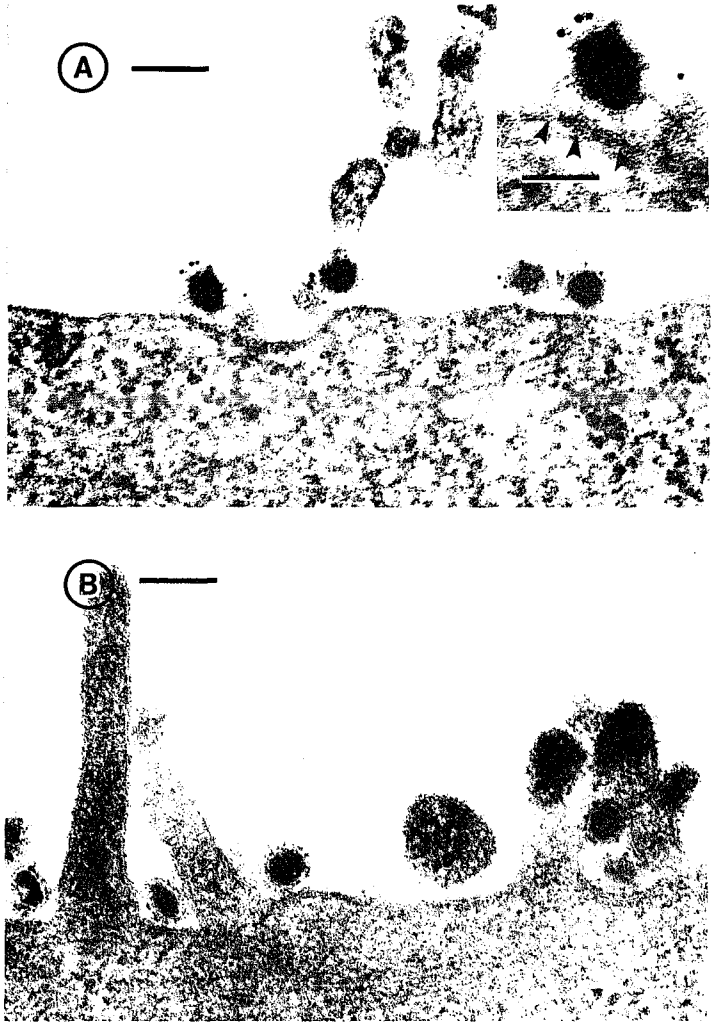

FIG. III.1. Immunoelectron microscopy of BCV interaction with the plasma membrane at 4°C. (A) Virus particles are labeled with gold. Envelope projections contact the cell membrane (inset, arrowheads). (B) Gold particles failed to bind to virions in preparations incubated with normal rabbit serum IgG. Bars = 100 nm, inset bar = 50 nm.

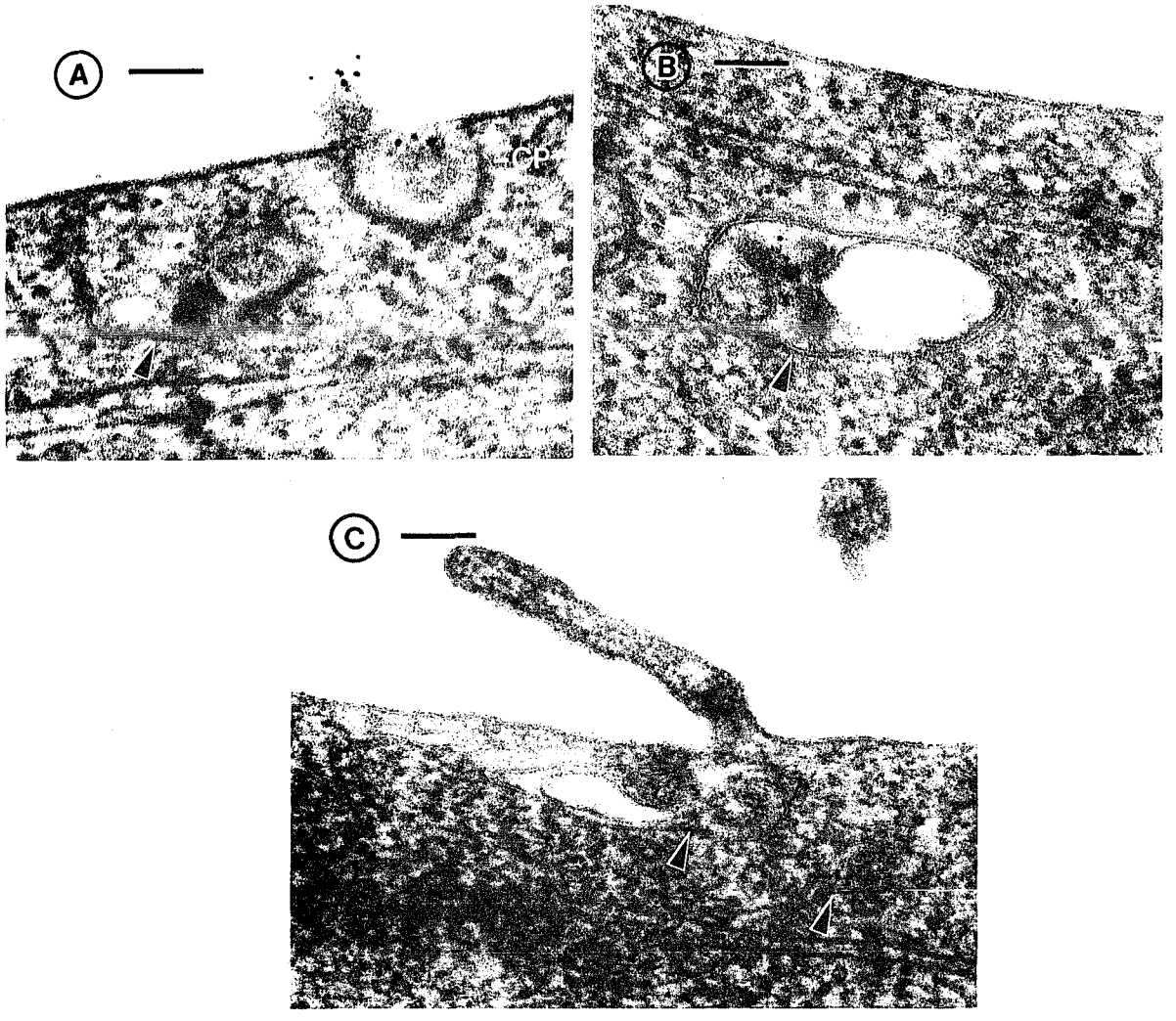

FIG. III.2. Early stages of BCV internalization. Monolayers were warmed for 2 min (A) or 5 min (B,C). Immunogold labeled virus particles are found in a coated pit (CP) and in intracellular vesicles with smooth membranes (arrowheads). Bars = 100 nm.

whereas the small smooth membrane vesicles were typically larger (160- to 300-nm in the greater dimension) and had diversely shaped profiles. These early membranous compartments usually contained only one or two virus particles but had very little empty space and few nonviral contents. After 10 to 15 min incubation at 37^{0}C, the intracellular virions accumulated in larger vacuoles, 400- to 800-nm across (FIG. III.3). These vacuoles contained as many as 10 labeled virions although some degeneration of particle morphology had occurred. The large vacuoles also contained unlabeled vesicles, fibrillar strands, and amorphous material. These latter contents indicate that the vacuoles may represent secondary lysosomes.

Gold particles were closely associated with virus structures and were separated from the nearest limiting cellular membrane by distances exceeding 20 nm. In a few cases, associations between gold particles and vesicle membranes were seen indicating possible intracellular sites of fusion (Fig III.3). The presence of a nearby virion or electron dense material made identification of the gold binding site ambiguous. After rewarming, gold particles were observed at plasma membrane sites distant from adsorbed virions (FIG. III.4). Apparent fusion of the virus envelope with the plasma membrane was recorded (FIG. III.5) but fusion of gold labeled virions with intracellular membranes was never observed.

Control experiments were conducted to confirm the specific nature of the gold marking of BCV antigens. Cells with surface-adsorbed virus that were incubated with normal rabbit IgG instead of anti-BCV antibody were not labeled by the gold probe (FIG. III.1B). Furthermore, gold

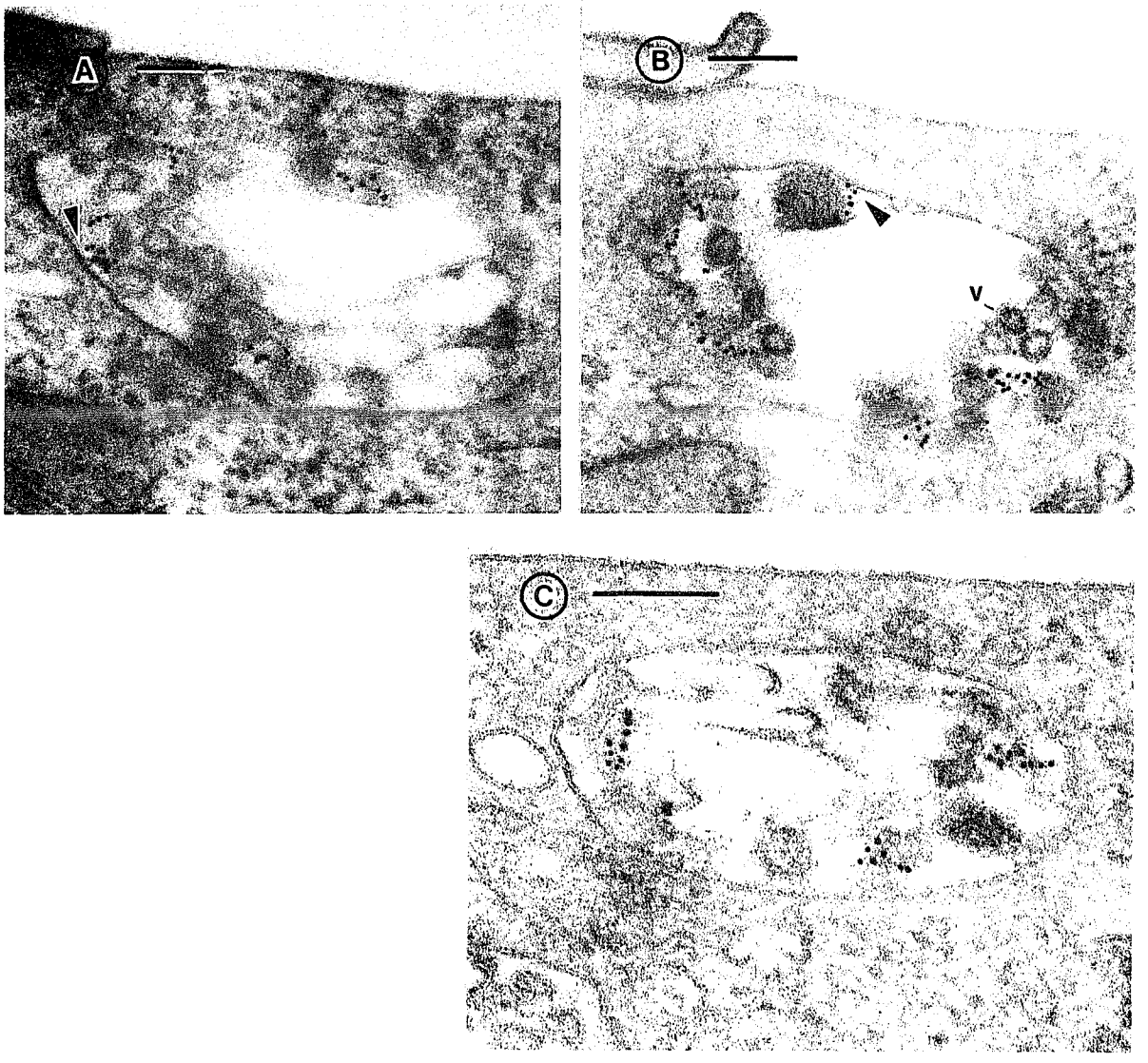

FIG. III.3. Accumulation of BCV inside vacuoles. Virus-cell complexes were incubated for 10 min (A) or 15 min (B,C) at 37^{0}C. Electron dense particles associated with gold represent partially degraded virions. Vacuole contents also include unlabeled vesicles (v) and fibrillar debris. Note possible sites of gold association with vacuole membranes (arrowhead). Bars = 100 nm.

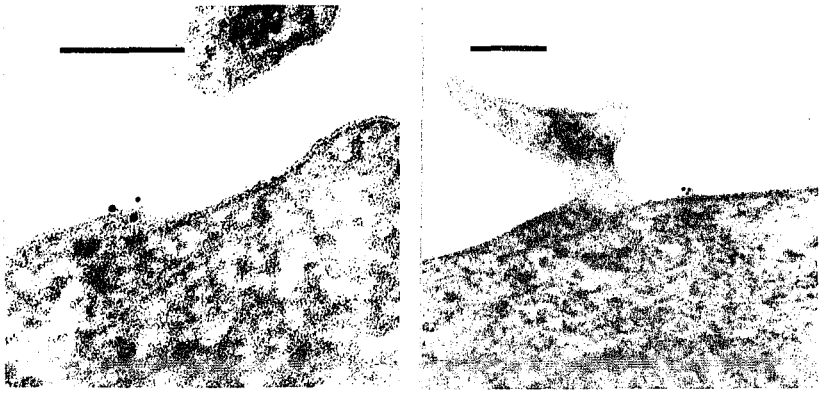

FIG. III.4. Association of gold label with plasma membrane after brief rewarming. Possible sites of viral envelope fusion with the plasma membrane are marked by gold particles. Bars = 100 nm.

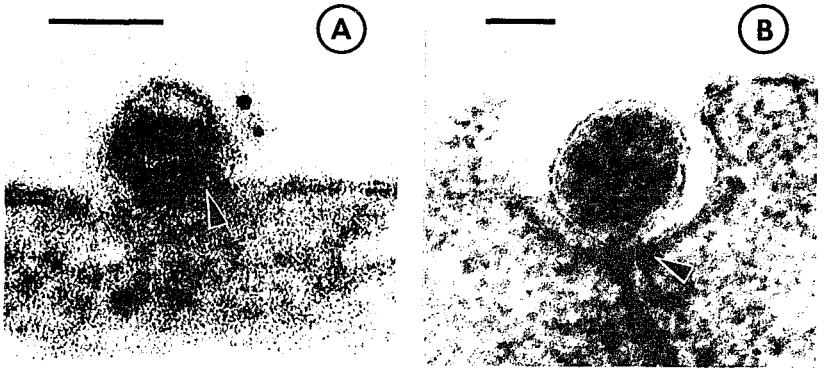

FIG. III.5. Interaction of BCV envelope with plasma membrane. Virus-cell complexes were rewarmed for (A) 30 sec or (B) 5 min. Note sites of apparent fusion marked by arrowheads. The virion depicted in B is unlabeled because the preparation was not incubated with immunoreagents. Bars = 50 nm.

particles were not observed at plasma membrane sites in the absence of virus particles when virus-cell complexes were immunolabeled and fixed at 4°C. These controls indicated that the immunoreagents specifically marked BCV antigens and not HRT-18 cell membranes.

III.C.3. Effect of lysosomotropic agents on the yield of infectious virus. We examined the effects of several lysosomotropic weak bases on BCV infection. These agents alter the pH of endocytic vacuoles and prevent endocytic entry by some other enveloped viruses. To compare the agents, synchronously infected cells were treated with chloroquine, amantadine, ammonium chloride or methylamine (Table III.1) at concentrations previously found to be effective in studies of virus entry (447, 61, 92, 101).

Table III.1. Effect of lysosomotropic agents on BCV infection

	Virus yield[a]		
Inhibitor (conc, mM)	Full Exposure	Delayed Exposure	%Reduction[b]
Ammonium chloride (10)	15 (7.02)	23 (7.20)	34
Methylamine (10)	15 (6.53)	24 (6.73)	37
Amantadine (0.5)	5.5 (6.09)	7.0 (5.90)	22
Chloroquine (0.12)	0.1 (3.87)	6.5 (5.72)	99

[a]Virus yield listed as percent of the positive control and as log PFU per ml (in parentheses).

[b]Percent reduction calculated as (1.0 - [full exposure/delayed exposure]).

Ammonium chloride, and methylamine at concentrations of 10 mM were relatively weak inhibitors of BCV infection when these agents were present throughout the infection. The presence of these agents during the first hour of infection produced less than a 40% decrease in BCV yield. Amantadine was a stronger inhibitor of the yield of infectious BCV in HRT-18 cells. An inhibitory effect was also seen in control preparations that were not exposed to the base during the first hour of virus replication. Additional exposure to amantadine for the first 60 min of infection resulted in only a 22% drop in virus yield. Thus, only chloroquine, of the four lysosomotropic agents tested, strongly suppressed the early stages of BCV replication. Infected cells that were fully exposed to 120 uM chloroquine from the time of synchronous infection until harvest produced only 1.4% as much virus as did cultures treated with chloroquine from 1 h post infection until harvest.

We tested the effects of various doses of ammonium chloride and chloroquine on BCV infection. Synchronously infected monolayers were exposed to the agents at the time of temperature shift to avoid drug effects on the virus adsorption stage. A second set of monolayers was pretreated with the drugs for 15 min and infected at 37^{0}C to insure that intravacuolar pH levels were altered during BCV entry. The effects of the agents were similar for both infection protocols. In synchronously infected cells, ammonium chloride reduced the yield of BCV by less than 1 log unit even at 20 mM levels (FIG. III.6A). The control treatment accounted for 90% of the reduction of virus yield by

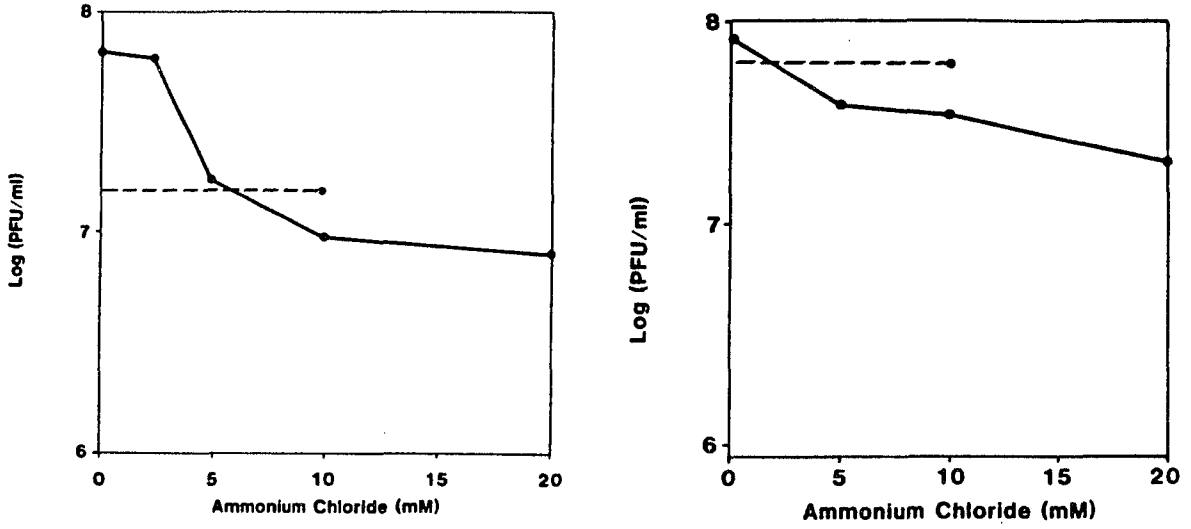

FIG. III.6. Effects of ammonium chloride on BCV yield by HRT-18 cells (A) synchronously infected with virus and (B) infected with virus at 37°C. Dashed lines represent virus yield when 10 mM ammonium chloride was added at 1 h post infection.

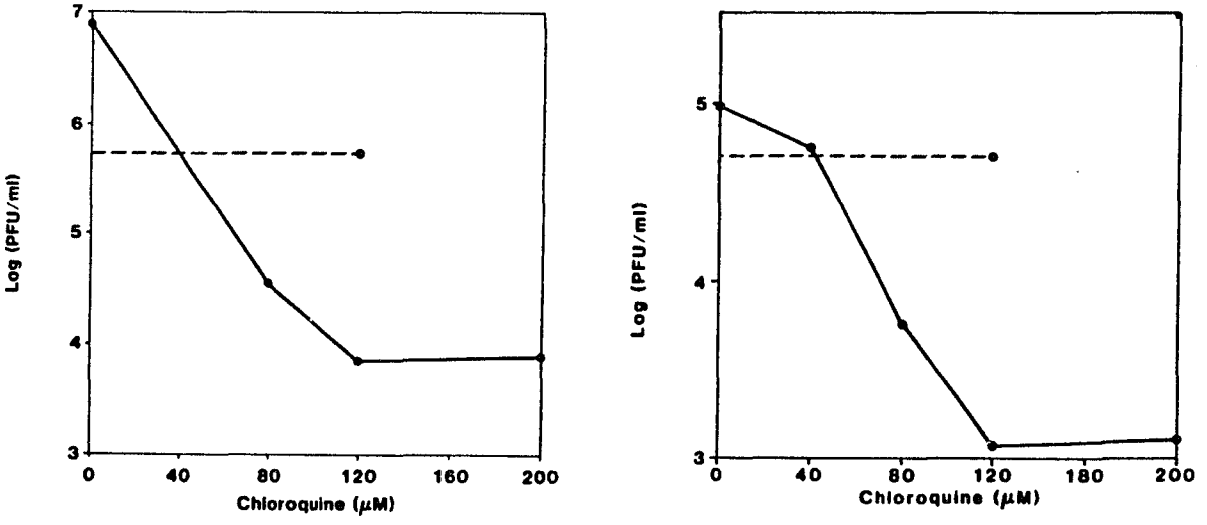

FIG. III.7. Effect of chloroquine on BCV yield by cells (A) infected synchronously and (B) infected at 37°C. Dashed lines represents virus level when 120 uM chloroquine was added at 1 h post infection.

10 mM ammonium chloride. A similar unresponsiveness to ammonium chloride treatment occurred during infection at 37^{0}C. The pretreatment with 10 mM ammonium chloride caused only a 37% decrease in BCV from levels produced when the agent was added after a 1 h delay (FIG. III.6B). However, 80 to 200 uM chloroquine strongly inhibited synchronous infection by BCV (FIG. III.7A). Cells pretreated with this agent and infected at 37^{0}C also produced less virus in response to increasing concentrations of the inhibitor (FIG. III.7B). The optimal inhibitory concentration of chloroquine, in terms of the difference between virus levels resulting from full and delayed treatment experiments was 120 um. Concentrations of the drug higher than 200 uM, when treatment was delayed for 1 h, diminished total virus yield to nearly the levels obtained by pretreatment. The inhibitory effect of 120 uM chloroquine on the early stages of BCV replication was therefore examined more closely in subsequent experiments.

III.C.4. Chloroquine inhibition of viral antigen production in infected cells. Immunofluorescence studies revealed that chloroquine treatments also affected the number of BCV-infected cells in HRT-18 monolayers (Table III.2). Treatments of synchronously infected cultures greatly decreased the number of fluorescent, antigen producing cells at 12 to 36 h post infection. Replication of BCV occurred in 10% to 17% of the cell population in untreated cultures. Only 1% or less of the cell population produced BCV antigens when exposed to chloroquine at the time of infection. The numbers of fluorescent cells in the monolayers reached nearly normal levels when

this treatment was delayed for 1 h even though cell vacuolization was pronounced.

Table III.2. Chloroquine effect on antigen production

Drug Exposure	%Fluorescing cells[a] 12 h	18 h	36 h
None	10	17	10
Full	1	0	1
Delayed	9	5	11

[a]Fluorescent cell population expressed as percent of total at indicated times post infection.

III.C.5. Time dependence of sensitivity to chloroquine inhibition. The time point for the early replicative step susceptible to chloroquine inhibition was more precisely determined (FIG. III.8). Synchronously infected monolayers were treated with chloroquine at various times post infection. Virus yields remained at low levels in cultures exposed to the drug at 5 min or less. Exposure to chloroquine at 10 min post infection reduced virus yield by more than 75%. Inhibition at 50% of maximum occurred with a treatment delay of approximately 15 min. These results indicate that 5 to 10 min were required for BCV replication to proceed beyond the chloroquine sensitive step.

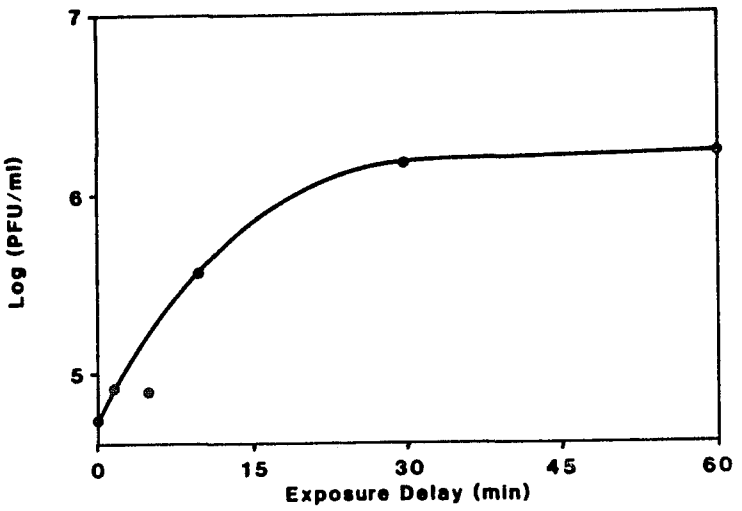

FIG. III.8. Time dependence of chloroquine inhibition of BCV infection.

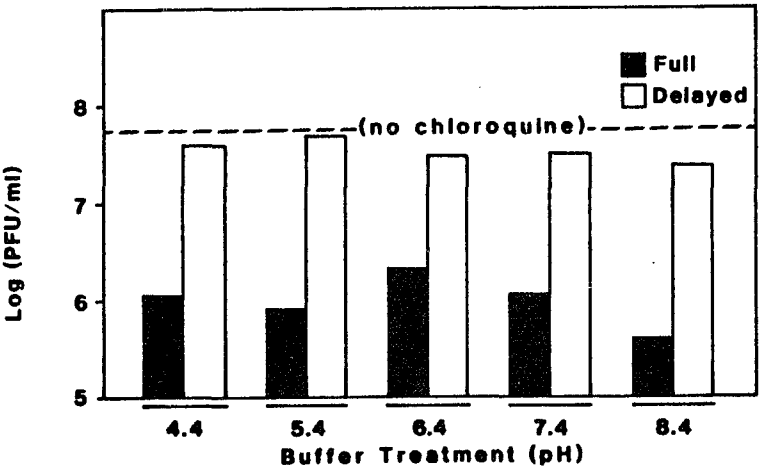

FIG. III.9. Independence of chloroquine inhibition to pH treatments.

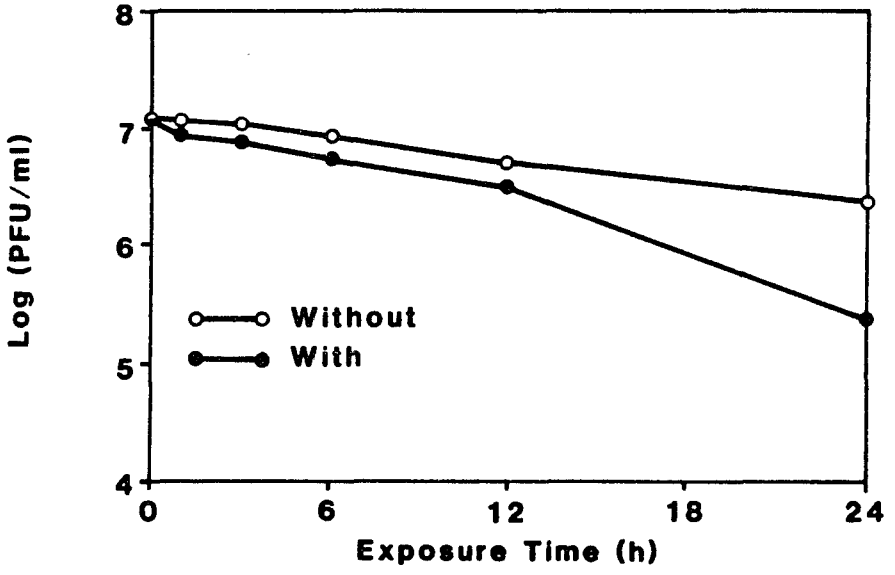

FIG. III.10. Effect of chloroquine on infectivity of BCV particles.

III.C.6. Independence of chloroquine inhibition to pH treatments. In an attempt to overcome the chloroquine imposed block in BCV entry, we tried to stimulate fusion between the plasma membrane and envelopes of infecting virions. Monolayers with virus adsorbed at 4^{0}C were exposed to chloroquine and briefly treated with warm buffers at various pH levels to simulate conditions in intracellular vacuoles. We found that chloroquine was an effective inhibitor of BCV infection despite buffer treatments in the range of 4.4 to 8.4 (FIG. III.9).

Direct effects of chloroquine on HRT-18 cell viability or on BCV infectivity were apparently not responsible for the inhibition. Each of the four lysosomotropic agents caused cytological changes in HRT-18 cells characterized by the development of large cytoplasmic vacuoles. With 120 uM chloroquine treatment, vacuolization began within three hours after exposure and reached maximum development after 12 hours. After 20 hours of treatment, however, cell viability remained as high as 90%. Furthermore, chloroquine treatment of infective BCV particles had little effect on the rate of inactivation during the first twelve hours of exposure (FIG. III.10).

III.D. DISCUSSION.

Many aspects of the initial stages in virus infection are disputed because current knowledge of this subject is in a primitive stage (32). Recent investigations have re-examined the role of endocytosis in infections by several animal viruses. Morphologic analyses have generally indicated that coronaviral entry is

accomplished by endocytosis (18, 25, 26, 107); yet other investigations have suggested that coronaviruses enter the cell by direct fusion with the plasma membrane (34). One of the objectives of our study was to employ immunolocalization to investigate the entry pathway for BCV.

Electron microscopic analysis confirmed that BCV particles were endocytosed by HRT-18 cells. Shortly after warming, the virus particles were seen in coated pits and in small endocytic vesicles with smooth membranes. The particles accumulated later in structures that appeared to be secondary lysosomes. Fusion of the viral envelope with the plasma membrane was observed but we were never able to find clear morphologic evidence of membrane fusion events along the intracellular membranes. This evidence indicates that BCV may effect infectious entry by direct fusion at the cell surface.

Experiments with lysosomotropic weak bases were conducted to identify a requirement for an acidic compartment during BCV entry. Such a requirement would support the endocytic pathway for infectious entry of this virus. Our results indicate that an acidic compartment is not required for BCV entry into HRT-18 cells and thus fail to support the endocytic pathway as an alternative route for infection. Ammonium chloride and methylamine were not inhibitory for events in the first hour of BCV replication. Although amantadine treatment from the time of infection reduced virus yield, the agent was also toxic when added after a 60 min delay.

Chloroquine interfered with an early stage of BCV replication as determined by the yield of infectious virus and by the number of BCV-infected cells. This effect apparently did not involve inhibition

of viral envelope fusion with cell membranes. The kinetics of time dependence for chloroquine inhibition suggests that the sensitive step in BCV replication occurs beyond 5 min post infection (FIG. III.7A). Addition of chloroquine as late as 10 min inhibits replication substantially (75%). In contrast, Semliki forest virus, which enters the cell by the endocytic pathway, procedes beyond the chloroquine sensitive phase within 4 min after infection and later treatments with the base are relatively ineffective (47).

Brief treatment of Semliki forest virus-adsorbed cell cultures with low pH media circumvented the chloroquine block apparently by allowing virus fusion at the plasma membrane (47, 158). The chloroquine blocked step in BCV infection was essentially unaffected by pH treatments in the range of 4.4 to 8.4. The failure of such treatments to relieve the chloroquine block in BCV replication may have several explanations. Plasma membrane fusion with BCV may not be triggered by low pH treatments. Other studies in our laboratory indicate that this is the case for BCV-infected bovine fetal spleen cells were pH 8 is optimal for cell fusion induced by this virus (H. R. Payne and J. Storz, manuscript in preparation). Cell fusion induced by a murine coronavirus also occurs optimally at a slightly basic pH (138). A second possible reason for a continued chloroquine block despite low pH treatment is that inhibition may involve events in replication subsequent to fusion. Studies of Sindbis virus infection have concluded that chloroquine inhibits only postfusion events in the replication of this virus (13). In those experiments, the antiviral

activity of the inhibitor was found to result from an effect on viral RNA synthesis rather than a block in Sindbis virus entry into the cell.

Our data indicate that BCV infection does not involve the endocytic route. Endocytosis of this virus appears to represent an abortive infection with subsequent virus degradation in lysosomes. The virions that were endocytosed were not observed to fuse with the vesicle membranes. Instead, the particles accumulated in a somewhat degraded form in lysosome-like structures. Furthermore, a low pH compartment is apparently unnecessary for BCV infection and virus-induced membrane fusion seems to be an event independent of low pH treatments. These features suggest that BCV infects cells by direct fusion with the plasma membrane. Doughri, et al. (34) observed interactions of BCV strain LY-138 with the plasmalemma of infected intestinal epithelial cells and asserted that virus uptake had occurred by direct fusion with the plasma membrane. Our studies provide evidence to support that conclusion.

CHAPTER IV: EXPRESSION OF BOVINE CORONAVIRUS ANTIGENS AT THE PLASMA MEMBRANE OF INFECTED CELL CULTURES

IV.A. INTRODUCTION.

Bovine coronavirus (BCV) is associated with many cases of enteric disease of viral etiology in newborn calves (54). The large, enveloped virions contain a positive sense RNA genome and are surrounded by a fringe of characteristic club-shaped peplomers. Five to eight immunogenic polypeptides, one of which is internal, have been reported for BCV virions (62, 63, 78, 130). The major envelope-associated polypeptides of coronaviruses are glycosylated and carry the structural sites responsible for hemagglutination and virus-cell interactions (20, 63, 136).

Coronaviruses usually exhibit limited cell and species tropisms. For this reason, apparently, the initial isolation of field strains of BCV is most successful in the human adenocarcinoma cell line HRT-18. Monolayers of these polarized epitheliod cells structurally resemble enterocytes -- the type of cells targeted by BCV in natural infections (33). Cultures of bovine fetal spleen (BFS) cells can also support the multiplication of the cell-adapted strain of BCV (96). Unlike HRT-18 cells, BFS cells are highly susceptible to BCV-induced cell fusion if trypsin is added to the medium of the infected culture (135). This phenomenon, known as fusion from within, suggests that the viral fusion factor is present at the surface of infected cells (160). Viral proteins in the host plasma membrane are not necessary for BCV maturation, however, because coronaviral particles are enveloped only

by budding into intracellular compartments (136). Viral components at the cell surface may contribute to intracellular spread of the infection and may also serve as targets for immune attack.

In this report, we describe the use of immunoelectron microscopy to characterize the appearance of BCV proteins in the plasma membrane of the host cell.

IV.B. MATERIALS AND METHODS.

IV.B.1. Cells and virus. Monolayers of the human rectal tumor cell line HRT-18 (145) were maintained in Dulbecco modified Eagle medium (DMEM) buffered with 44 mM $NaHCO_3$ and supplemented with 5% fetal calf serum. The D2 strain of BFS cells was maintained in minimal essential medium (MEM) buffered with 25 mM HEPES and supplemented with 10% fetal calf serum. Stock preparations of the Mebus strain L9 of BCV (121, 131) were propagated in HRT-18 cells. Virus stocks were generated from cells infected at a multiplicity of approximately 0.01 PFU per cell, incubated for 4-5 days at 37^{0}C in serum-free DMEM and harvested by freeze-thawing. Viral titers obtained in these preparations ranged from 10^6 to 10^7 PFU per ml.

IV.B.2. Infection of cell cultures. Monolayers for immunogold labeling experiments were grown in 20 cm^2 solvent-resistant culture dishes and monolayers for immunofluorescence studies were cultivated in multiwell chamber slides (Miles Scientific). HRT-18 cells were washed with DMEM, and infected with BCV for 60 min at 37^{0}C at a multiplicity of approximately 1.5 PFU per cell. The cultures were fed with fresh

DMEM and incubated at 37°C in a 5% CO_2 atmosphere. In a similar manner, monolayers of BFS cells were washed with MEM and infected with BCV at a multiplicity of 20 PFU per cell. Infected BFS cultures were maintained in MEM with and without the addition of 0.2 ug/ml of trypsin which contained tolylsulfonyl phenyalanyl chloromethyl ketone to inhibit chymotrypsin activity (Sigma Chemical Company). At various times post infection, cultures were removed from the incubator and fixed at 4°C for immunolabeling.

IV.B.3. Indirect immunofluorescence. Infected monolayers were fixed for 10 min in 4% formaldehyde in 0.01 M NaPO4, 0.14 M NaCl, pH 7.3 (PBS), with 0.005% $CaCl_2$ and 0.11 M sucrose, permeabilized for 5 min with acetone at -20°C, incubated with rabbit anti-BCV antibody, and reacted with goat anti-rabbit antibody conjugated to fluorescein isothiocyanate. The preparations were viewed with a Leitz fluorescent microscope using epifluorescence.

IV.B.4. Immunogold localization. Cell monolayers were fixed for 30 min at 4°C in 1% glutaraldehyde in PBS, pH 7.3, and washed overnight in PBS followed by a 10 min treatment with 1mM glycylglycine. The fixed monolayers were labeled at 4°C by an incubation in rabbit anti-BCV IgG followed by an incubation with goat anti-rabbit:colloidal gold complex. Infected control monolayers were incubated with normal rabbit IgG instead of anti-BCV antibody.

IV.B.5. Processing for electron microscopy. The gold labeled monolayers were fixed again in 1% glutaraldehyde in PBS for 1 h at 25°C, incubated for 1 h in a solution of 1% osmium tetroxide and 1% potassium ferrocyanide in PBS, washed in 0.2 M sodium acetate buffer, pH 3.5, and stained *en bloc* for 1 h with 0.2% uranyl acetate in acetate buffer. After washing in distilled water, the cells were dehydrated in an ascending alcohol gradient, embedded *in situ* in Spurr's epoxy resin (129), and polymerized at 60°C. The embedded monolayers were peeled from the plastic substrate, reembedded, and oriented so that thin sections were cut perpendicular to the monolayer plane. The thin sections were stained with uranyl magnesium acetate followed by lead citrate and viewed with a Zeiss EM-10 electron microscope at 80 kV.

IV.B.6. Immunoreagents. Rabbit antiserum to BCV that had been purified from infected bovine fetal kidney cells was prepared by previous investigators in our lab. The antibody level was titered by a plaque neutralization test. The IgG fractions of the antiserum and of normal rabbit serum were obtained by protein A-sepharose column chromatography. Goat anti-rabbit antibody (IgG) complexed to 5-nm colloidal gold particles (Janssen Life Sciences Products, Beerse, Belgium) was used. The immunoreagents were diluted in PBS containing 0.5% goat serum.

IV.C. RESULTS.

IV.C.1. Expression of BCV antigens in HRT-18 cells. We selected the HRT-18 line as host cells for study because these cells share

distinctive morphological features with absorptive cells of the intestinal mucosa. Virus-specific fluorescence was observed in approximately 10% of the cell population at 12, 24, and 36 h after infection (FIG. IV.1). The percentage of fluorescent cells in the culture increased little at the later times. We examined thin sections of immunolabeled HRT-18 cells to detect BCV antigens at the cell surface. Cells fixed prior to 9 h were not marked but the colloidal gold particles were observed at widely scattered locations on the apical surfaces of cells fixed at 12 h (FIG. IV.2). The surfaces of infected HRT-18 cells were abundantly labeled by 24 h (FIG. IV.3). The gold-labeled BCV antigens were located on both microvilli and on planar portions of the apical plasma membrane. The gold particles were separated spatially and clustering of BCV antigens in the membrane plane was not apparent. Typically, these densely labeled cells were surrounded by cells that were not marked by gold particles.

Control preparations included (i) uninfected HRT-18 cells that were incubated with anti-BCV antibody and (ii) infected cells that were incubated with the IgG fraction of normal rabbit serum. These cells were not labeled by the gold probe because the antibody bound only to virus-specific antigens. Additionally, in related studies, we observed that the plasma membrane is not labeled on uninfected HRT-18 cells adsorbed at $4^{0}C$ with BCV and incubated with these immunoreagents (Manuscript in preparation. H.R. Payne, W.G. Henk, and J. Storz). Therefore, binding of subviral components to cellular receptors did not contribute to the association of gold particles with the plasma membrane. Our attempts to use post-embedment techniques to identify

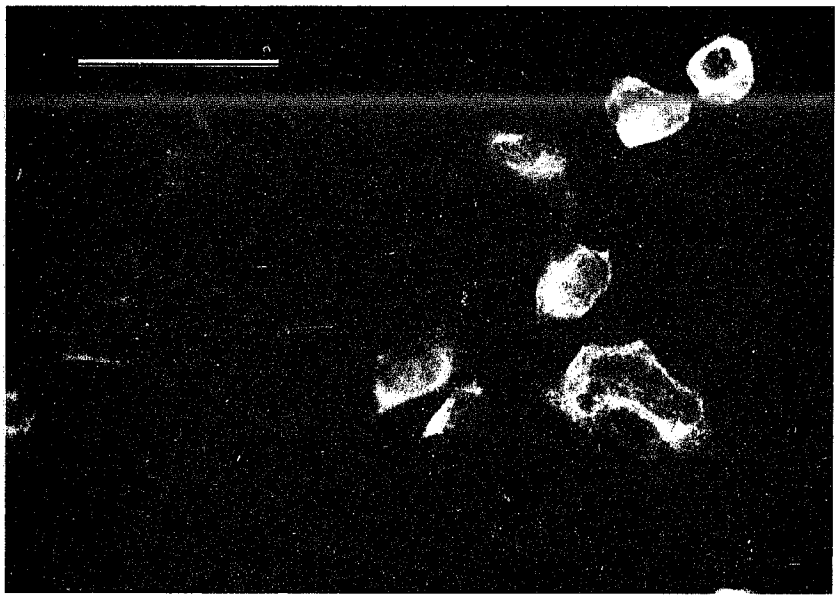

FIG. IV.1. Immunofluorescence of BCV antigens in infected HRT-18 cells at 24 h post infection. Bar = 50 um.

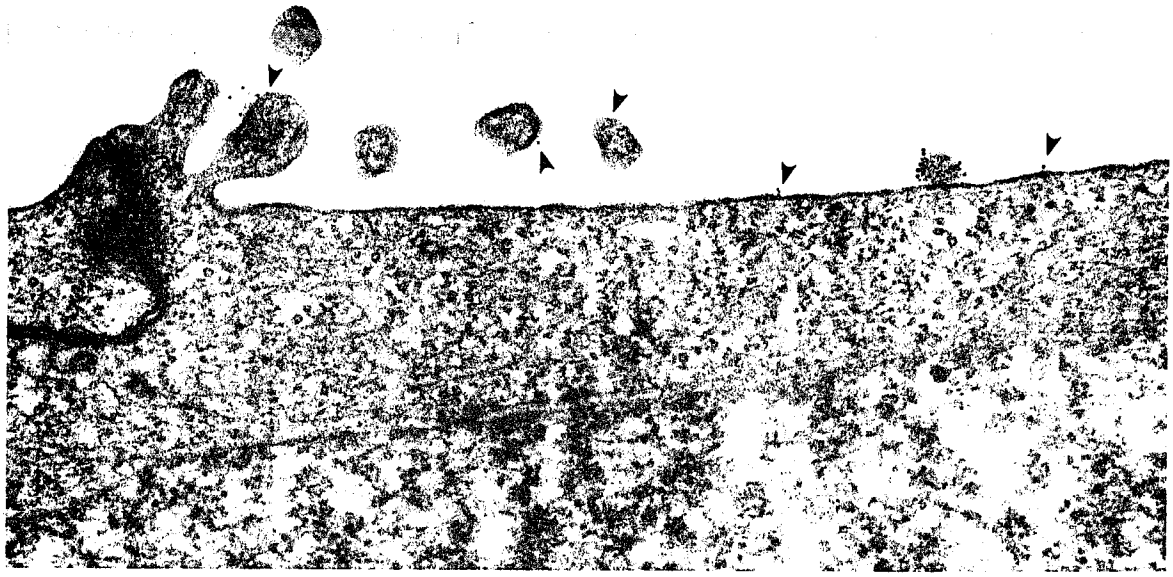

FIG. IV.2. Immunogold labeled HRT-18 cells at 12 h post infection with BCV. Locations of viral antigens are marked by gold particles (arrowheads). Bar = 200 nm.

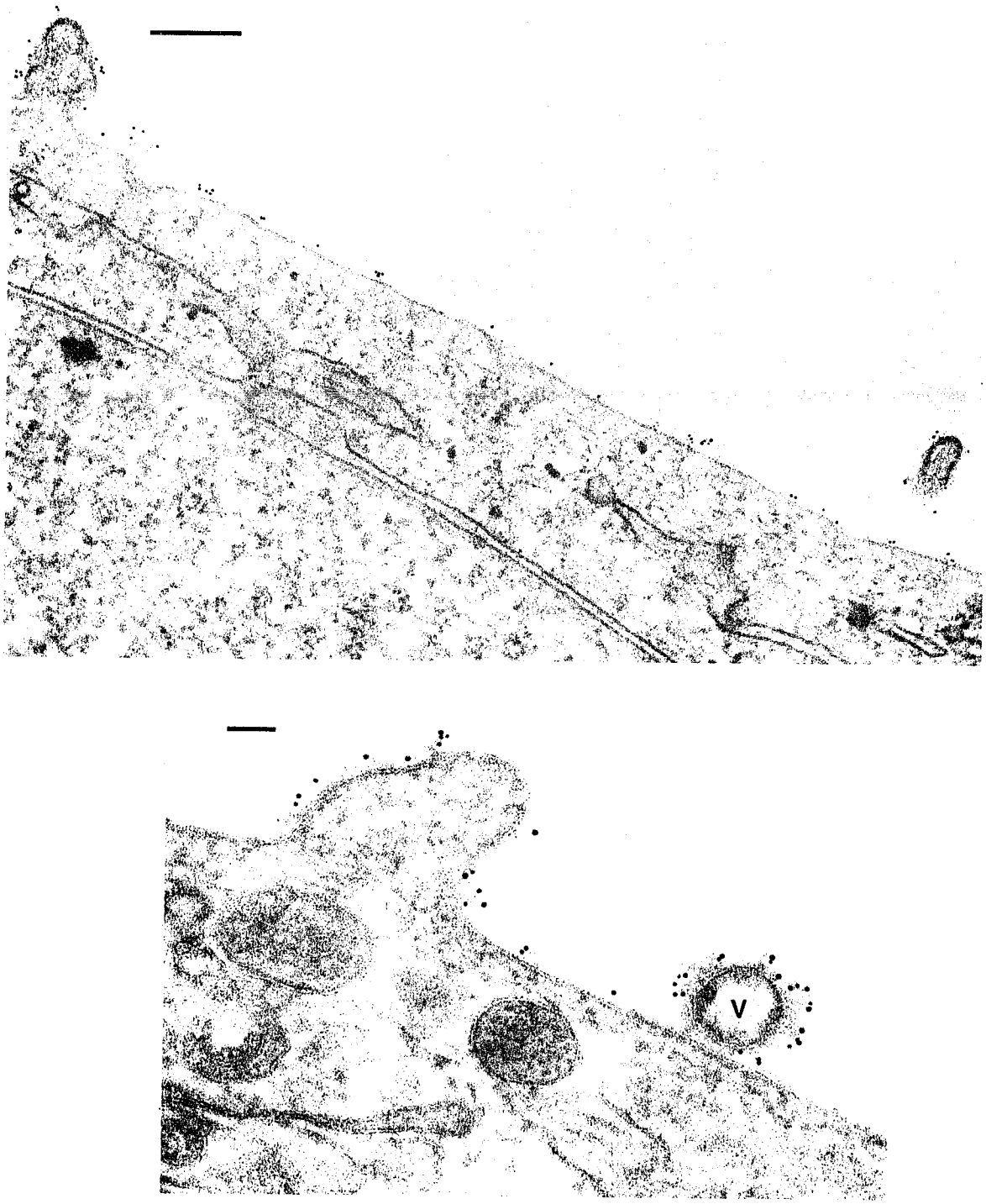

FIG. IV.3. Immunogold labeled infected HRT-18 cells, 24 h post infection. V, coronavirion. Bars = 200 nm.

viral antigens at basolateral aspects of the cell membrane were unsuccessful.

IV.C.2. Expression of BCV antigens in BFS cells. Fusion of BFS cells was induced by BCV replication when cultures were incubated in medium with trypsin (FIG. IV.4). Cell fusion was not observed in the absence of trypsin. The fusion process may contribute to intercellular spread of the infection by the recruitment of uninfected cells into enlarging polykaryons. We used immunofluorescence and immunogold electron microscopy to correlate observations of the onset of cell fusion with the development of viral antigens. Faint fluorescence was first recognized in the culture at 9 h post infection. Approximately 33% of the cell population fluoresced at 15 h (FIG. IV.5A). Cell fusion was initially evident at 18 h in cultures incubated with trypsin. These cultures contained large polykaryons with cytoplasmic fluorescence at 24 h (FIG. IV.5). Only mono- and bi-nucleated cells, of which 25% were fluorescent, were observed at 24 h in the absence of trypsin. Uninfected cells predominated in these cultures while fewer than 10% of the remaining single cells in trypsin-treated cultures were nonfluorescent at 24 h.

Electron microscopic observations revealed no evidence of cell fusion in BFS monolayers fixed after 15 h of infection in the presence of trypsin (FIG. IV.6A). The immunogold technique labeled multiple sites of BCV antigens in the plasma membrane at this time, however (FIG. IV.6B). At later times, trypsin treatment had no apparent effect on the abundance of labeled antigens at the cell surface (FIG. IV.7).

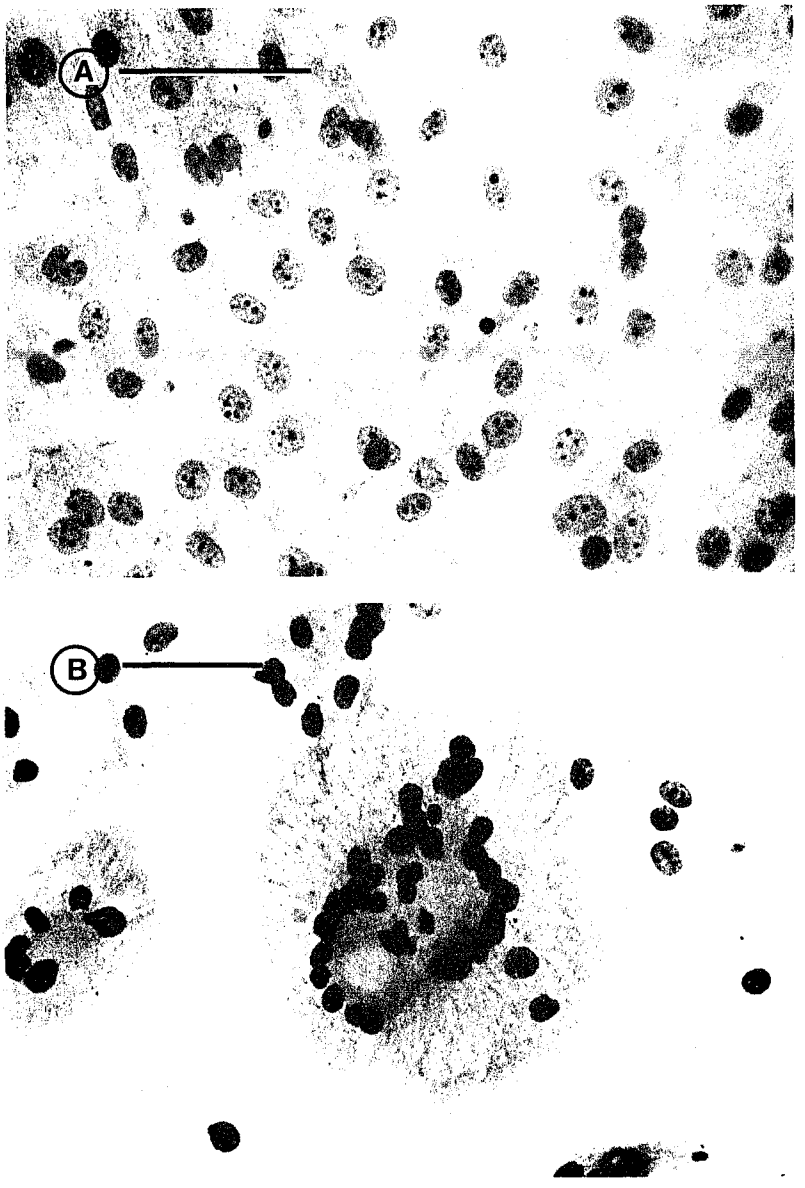

FIG. IV.4. Polykaryocytosis in virus infected BFS cells. (A) Cells incubated without trypsin did not fuse. (B) Polykaryons formed after 24 h incubation with trypsin. Giemsa stained preparations. Bars = 50 um.

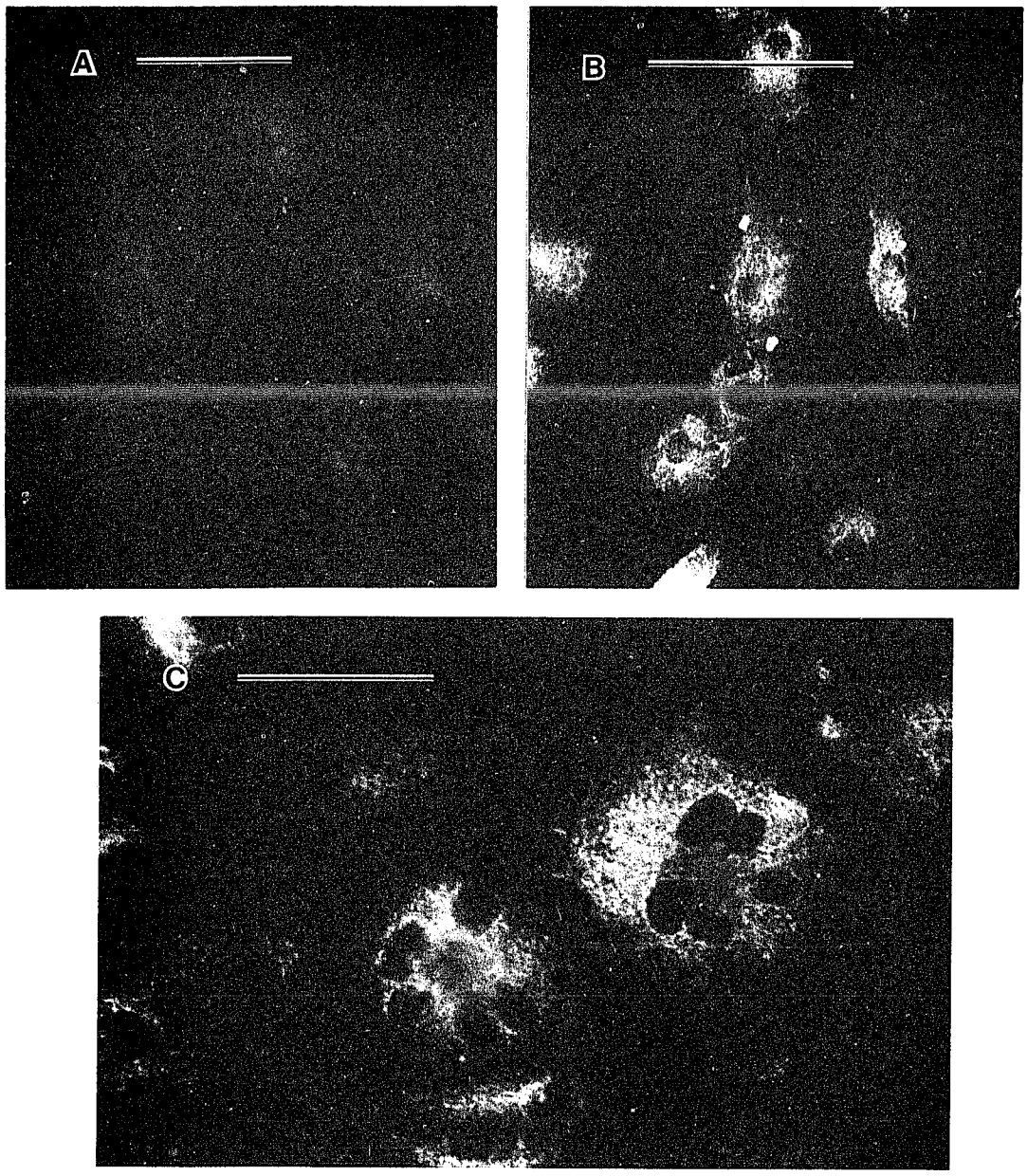

FIG. IV.5. Immunofluorescence of virus infected BFS cells at (A) 15 h post infection and (B,C) at 24 h post infection. Cultures in (A) and (C) were infected in the presence of trypsin. Bars = 50 um.

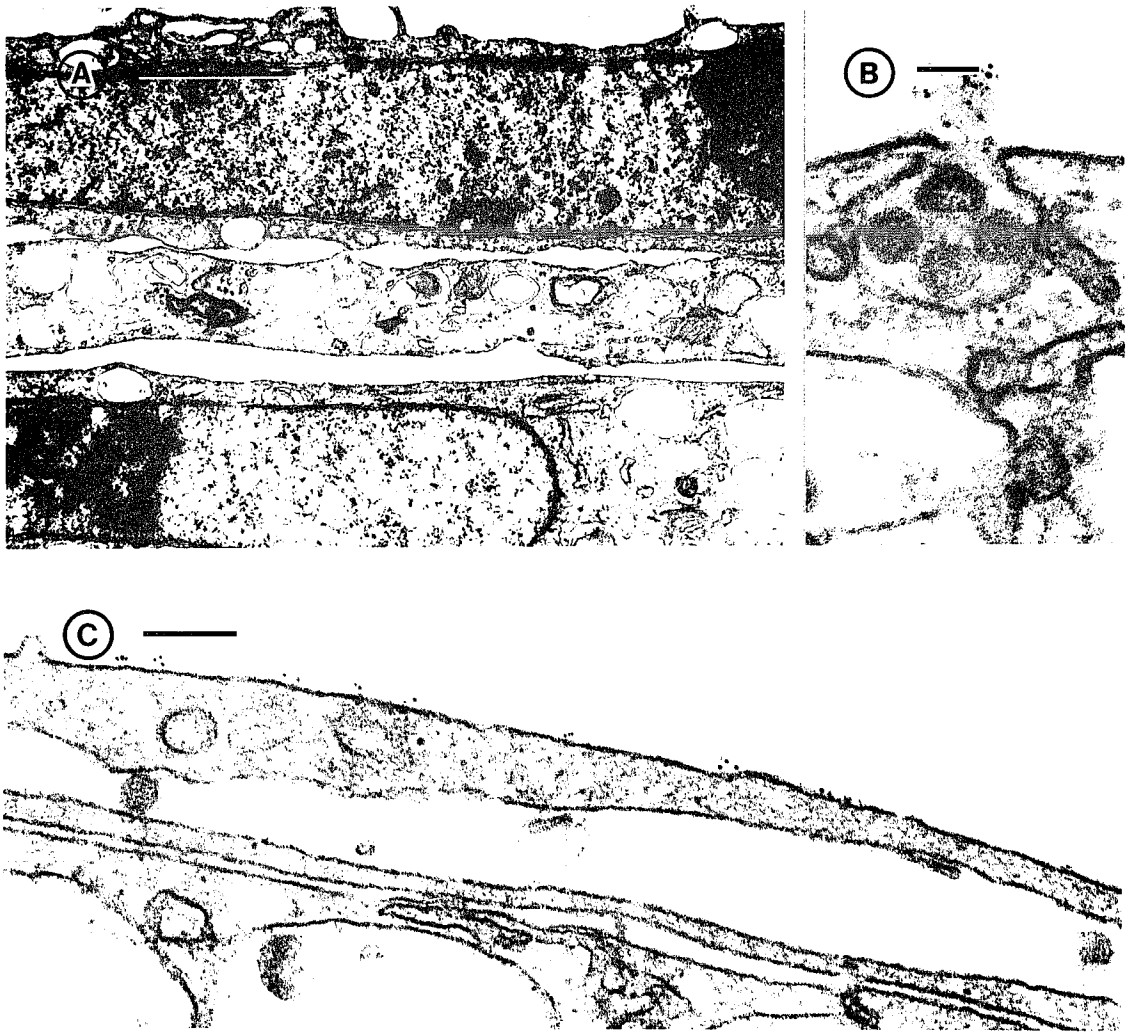

FIG. IV.6. Immunogold labeled BFS cells at 15 h post infection in the presence of trypsin. Bars = 1.0 um in (A) and 50 nm in (B) and (C).

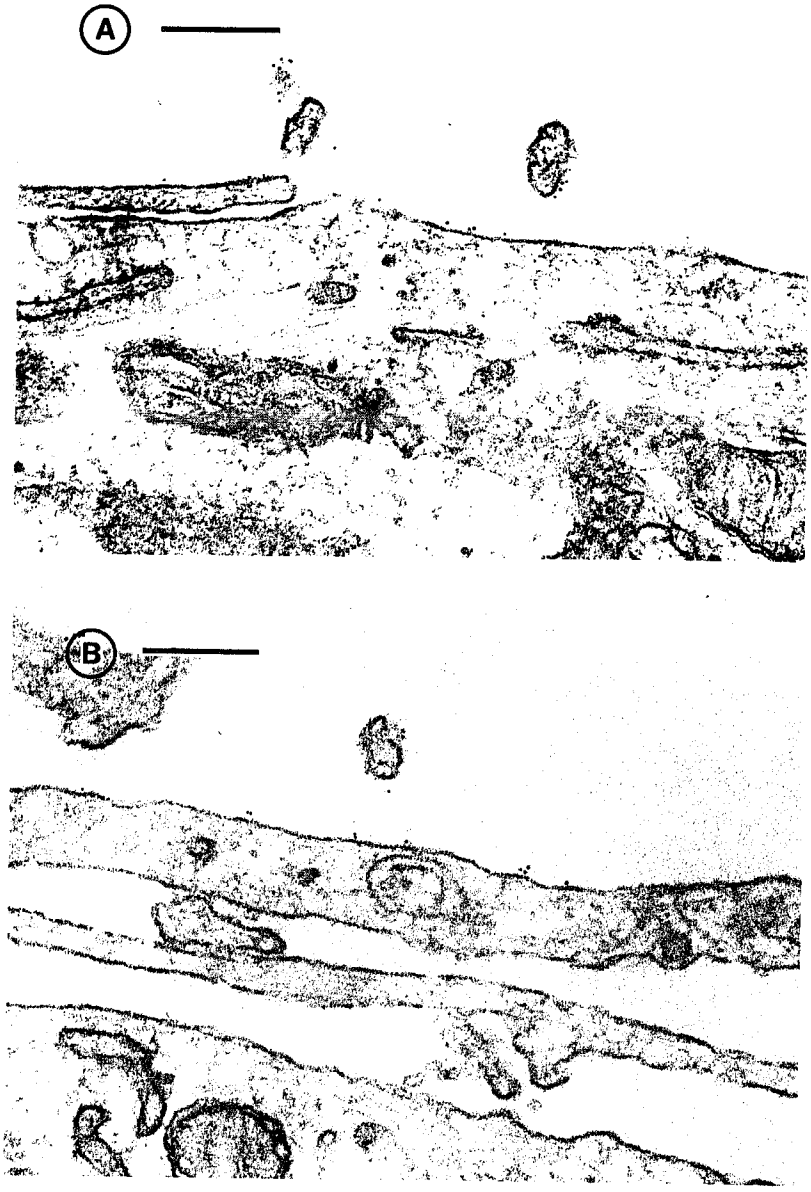

FIG. IV.7. Immunogold labeled BFS cells at 24 h post infection in the (A) presence and (B) absence of trypsin. Bars = 200 nm.

The number of gold binding sites on polykaryons at 24 h was approximately equal to that of cells not treated with trypsin.

IV.D. DISCUSSION.

We used immunolocalization techniques to probe morphological characteristics of BCV infection in an epitheliod cell line (HRT-18) and in bovine fibroblastic cells (BFS) which are highly susceptible to BCV-induced cell fusion. The envelopment of BCV occurs on intracellular membranes. Despite this intracellular mode of maturation, we demonstrated that BCV antigens are expressed at the surfaces of infected cells of both types. These immunogold-labeled surface antigens were found in areas free of attached virions. The immunogold technique labeled BCV antigens but did not label cellular antigens or cell-surface adsorbed subviral components in control preparations. Consequently, the sites at the cell surface labeled by gold represent de novo expression of virus-specific proteins in the plasma membrane.

Although HRT-18 monolayers were infected with BCV at a multiplicity of 1.5 PFU per cell, only a minority of these cells developed cytoplasmic fluorescence within 36 h. The large population of non-fluorescent cells probably were less susceptible to virus infection or were nonpermissive for synthesis of viral proteins. The frequent presence of immunogold-labeled HRT-18 cells in thin sectioned preparations adjacent to uninfected cells, free of the gold marker, support this interpretation. Viral antigens could first be

demonstrated in the apical plasma membrane by 12 h, but the antigens increased to higher density by 24 h.

Polykaryocytosis was evident by 18 h in infected BFS cells incubated in medium with trypsin. Following the onset of cell fusion in these cultures, the number of non-fluorescing BFS cells was reduced. Parallel cultures incubated without trypsin maintained a stable number of non-fluorescing cells. The decrease evidently resulted from the recruitment of uninfected cells into enlarging polykaryons. This process may relate to a cell-associated spread of the virus infection. The decreased number of non-fluorescent BFS cells also might result from an increased efficiency in the infection process resulting from trypsin activation of the fusion factor (130).

Infected BFS cells produced cytoplasmic BCV antigens within 9 h, and expressed viral antigens in the plasma membrane at 15 h in the presence of trypsin. Consequently, viral antigen appeared at the plasma membrane several hours prior to the onset of cell fusion which was first observed at 18 h. BFS polykaryons failed to accumulate more viral antigens in the plasma membrane after the onset of cell fusion. This surprising result contrasted with the progressive accumulation of viral antigens in infected HRT-18. The result could be caused by several possible differences between the infected cell types including (i) the kinetics of protein transport to the plasma membrane and (ii) the process of membrane recycling. When trypsin was omitted from the medium of infected BFS cells, antigens were expressed at the plasma membrane although cell fusion never occurred. This observation indicates that the action of trypsin in polykaryon formation involves

effects other than an increase in the number of viral antigens at the cell surface.

Coronavirus particles may be released by intact cells (51, 136) or by cytolysis of the infected cells (33, 34, 136). We observed virus particle-filled vesicles continuous with the plasma membrane as early as 15 h after infection in BFS cells (FIG. IV.6C). This event appears to represent exocytosis of newly formed coronavirus particles. Fusion of such vesicles with the plasma membrane would leave excess viral proteins at the cell surface and account for the appearance of antigens.

Our results are in agreement with reports of viral proteins at the surface of cells infected with mouse coronaviruses. Collins et al. (20) used immunoferritin electron microscopy to demonstrate that the 170,000 molecular weight (GP-1) protein of MHV-4 is present at the surface of infected L-241 cells at 6 h post infection. Other evidence for coronavirus-specific proteins at the cell surface has relied on inhibition of virus-induced cell fusion by antibodies specific for envelope proteins (52, 136, 138) and on fusion foci experiments (99, 146). Our immunogold procedure reveals the precise sites of coronaviral antigens in the plasma membrane and extends the earlier observations to include the bovine coronavirus.

The expression of BCV antigens in the plasma membrane has important implications for host-virus interactions aside from polykaryon formation. For example, appearance of virus-specific surface components during eclipse may render the infected cell susceptible to specific antibody-dependent or cell-mediated host

defense mechanisms. The infected cell could potentially be destroyed prior to the release of new virus.

CHAPTER V: ANALYSIS OF MEMBRANE FUSION INDUCED BY BOVINE CORONAVIRUS INFECTION

V.A. INTRODUCTION.

Infection of animal cells by enveloped viruses involves fusion between the viral envelope and a cell membrane. The fusogenic potential of viruses has been studied *in vitro* with systems using erythrocytes, cultured cells, and liposomes as target membranes (55, 57, 152, 159, 160). Membrane fusion is induced by paramyxoviruses at neutral pH thus these viruses may enter the host cell at physiological pH by fusing with the plasma membrane at the cell surface (reviewed in 19, 32). In contrast, the cell fusion activities of Semliki forest virus, influenza virus, and vesicular stomatitis virus are strictly dependent on acidic pH levels (37, 43, 158, 159). Low pH is used experimentally to simulate conditions existing within the acidic intracellular vesicles where penetration by these viruses is thought to naturally occur.

Cell fusion and polykaryon formation in cultures infected with bovine coronavirus (BCV) occur late in the virus replicative cycle. In many types of host cells, polykaryocytosis is dependent on the presence of trypsin during the course of BCV replication (135). The membrane events of virus-induced cell fusion and virus-cell fusion during entry appear to be based on the same principle (68) but the mode of BCV penetration of the host cell has not been reported. We studied the trypsin susceptibility of BCV-infected cells and found that fusion is optimal at pH 7.5 to 8.0. Our observation that alkaline conditions

support BCV-induced polykaryocytosis suggests that this virus may penetrate cells by direct fusion with the plasma membrane.

V.B. MATERIALS AND METHODS.

V.B.1. Virus and cells. Stock preparations of the Mebus strain L9 of BCV (121, 131) were propagated in the human rectal tumor cell line HRT-18 (145). Virus stocks were generated from cells infected at a multiplicity of approximately 0.01 PFU per cell, incubated for 4-5 days at 37^{0}C in Dulbecco modified Eagle medium (DMEM) buffered with 44 mM $NaHCO_3$ and harvested by freeze-thawing. Viral titers in these preparations ranged from 10^6 to 10^7 PFU per ml. The D2 strain of BFS cells was maintained in minimal essential medium (MEM) buffered with 25 mM HEPES and supplemented with 10% fetal calf serum.

V.B.2. Effects of trypsin and trypsin inhibitor on BCV replication. Monolayers grown in 25 cm^2 flasks were inoculated with BCV at a multiplicity of 2 PFU per cell, incubated at 37^{0}C for 60 min and washed with MEM. The cultures were incubated in MEM containing trypsin (0.4 ug per ml; Sigma Chemical Company) treated with tolylsulfonyl phenyalanyl chloromethyl ketone, an inhibitor of chymotrypsin activity. Trypsin-treated and untreated cultures were also exposed to soybean trypsin inhibitor (0.4 ug per ml; Sigma Chemical Company) during the period of trypsin treatment. After 24 h, the cultures were harvested by two freeze-thaw cycles and the material was disrupted by sound (Branson Sonic Power Company) for 30 sec on ice

to release the virus. Virus yields were determined by plaque assays and hemagglutination assays.

V.B.3. Virus-induced polykaryon formation. Monolayers of BFS cells were grown in 24-well plates washed with MEM and adsorbed for 1 h at 37°C with BCV at a multiplicity of 20 PFU per cell. The cultures were covered with MEM with and without the addition of 0.4 ug of trypsin per ml and incubated at 37°C. Exposure to trypsin activity prior to harvest was terminated by rinsing the monolayer once with MEM then adding MEM containing 0.4 ug of soybean trypsin inhibitor per ml. The cultures were incubated for 26 h of infection, fixed for 10 min in Bouin's fixative and stained with Giemsa. The cells were examined microscopically with a 25X objective and the extent of cell fusion was scored by counting the number of polykaryons with 4 or more nuclei in 5 randomly selected fields.

V.B.4. Effect of pH level on virus-induced fusion. Preliminary experiments were conducted to identify the time period in which BCV-infected BFS cells are susceptible to the presence of trypsin. Each infected monolayer was exposed to trypsin for a 1, 2, or 4 h interval during the period of virus replication. After 26 h, the monolayers were fixed, stained, and scored for polykaryon formation.

We then analyzed the effects of the pH level on polykaryon formation. The monolayers were infected as described above and incubated in MEM buffered with 10 mM HEPES and 10 mM MES at pH 7.0, 7.5, and 8.0 for 19 h at 37°C without trypsin. The cells then were

treated for 2 h at 37°C with 1.0 ug of trypsin per ml of MEM at various pH levels. The trypsin treatment was terminated and the monolayers were incubated for an additional 5 h in trypsin-free medium at pH 8.0 before fixation and staining.

V.B.5. Antibody suppression of cell fusion. The IgG fractions of the rabbit anti-BCV serum and of normal rabbit serum were obtained by protein A-sepharose column chromatography. The ability of anti-BCV IgG to affect polykaryon formation at 37°C was tested by two procedures: (i) Infected cell monolayers were incubated for 6 h in trypsin-free MEM then exposed to MEM that contained antibody freshly diluted with trypsin. These monolayers were fixed and stained after 18 h of infection. (ii) Monolayers were infected for 9 h then treated with antibody for 1 h in the absence of trypsin. The cells were covered with medium containing trypsin after the antibody treatment, incubated for an additional 8 h, and then fixed.

V.C. RESULTS.

V.C.1. Effects on trypsin and trypsin inhibitor on BCV replication. The presence of trypsin at some time during virus replication in BFS cells was an absolute requirement for the development of polykaryons under all conditions tested in this study. Cell fusion failed to occur in infected cultures without trypsin or when soybean trypsin inhibitor was present during treatment. BCV replication apparently proceeded unabated in the absence of trypsin. The addition of trypsin to infected cultures at 3 h increased the yield

of infectious virus by only 38% but the hemagglutination titer rose by 400%. Addition of trypsin inhibitor to infected cultures caused a small (39%) decrease in the yield of infectious virus but the hemagglutination titer was unaffected. These results suggest that treatment with either trypsin or trypsin inhibitor had no substantial effect on the yield of infectious virus during a single cycle of virus replication.

V.C.2. Replication period susceptible to trypsin. Experiments conducted to identify the period of infection susceptible to trypsin activation of fusion revealed that the onset of cell-to-cell fusion occurred at about 18 h post infection with continuous trypsin treatment. This treatment resulted in large multinucleated cells by 26 h (FIG.V.1). We found that a single trypsin treatment for an interval as brief as 1 to 2 h could result in the formation of polykaryons after 26 h. These polykaryons generally were smaller and contained fewer nuclei per cell than the fusion products of continuous trypsin treatment.

Intervals of trypsin treatment that ended prior to 14 h post infection produced less than 6% polykaryocytosis (FIG. V.2). The greatest numbers of polykaryons (74 to 124 per field) developed in monolayers treated for a 2 or 4 h interval during the period between 18 and 22 h post infection. This observation was used in subsequent experiments to determine the optimal pH level for cell fusion.

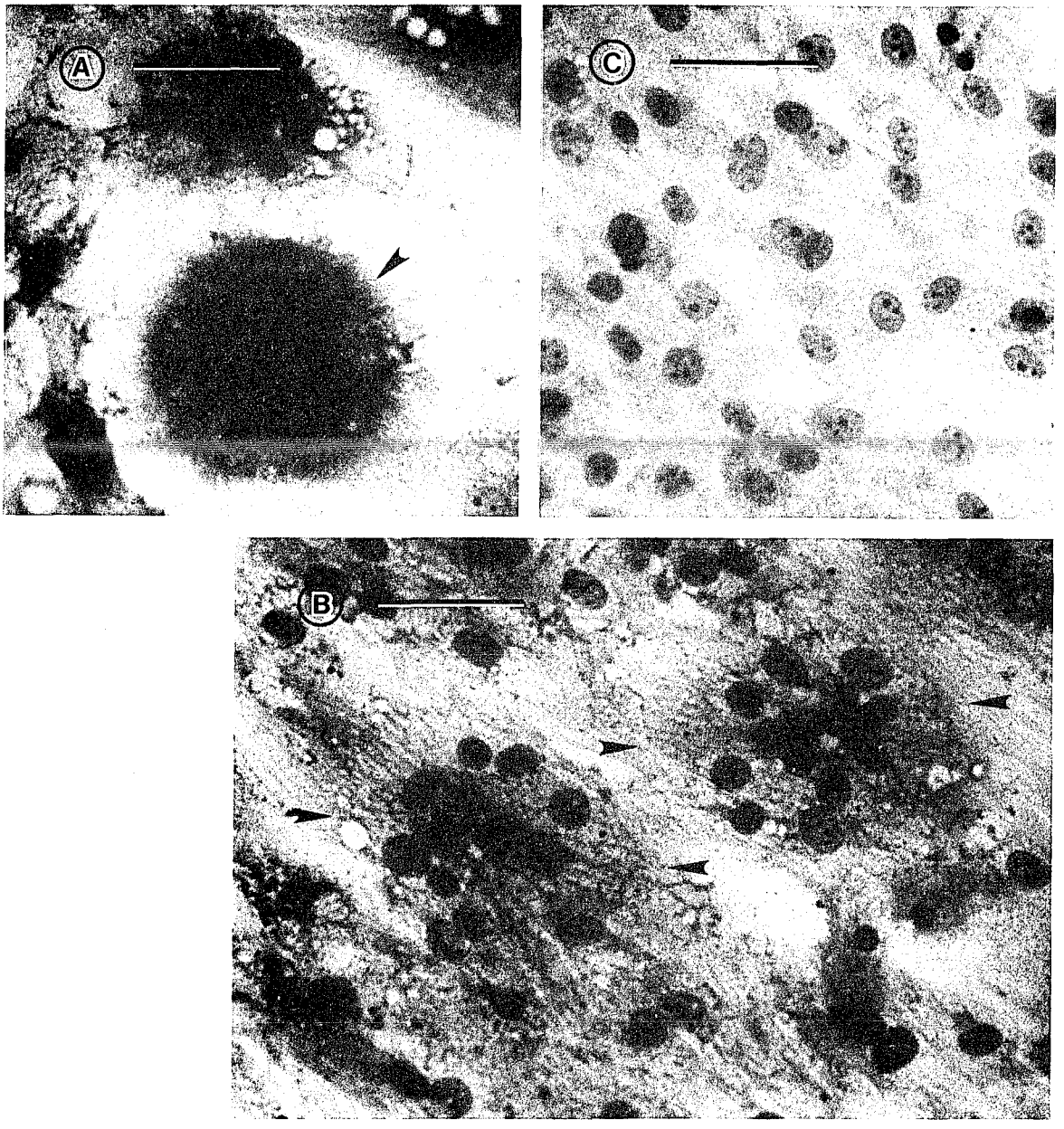

FIG. V.1. Polykaryon formation in BFS cultures infected 26 h with BCV. (A) Large polykaryons (arrowhead) develop in cultures treated continuously with trypsin. (B) Smaller polykaryons (arrowheads) develop when the trypsin treatment is limited to a 2 h period (20 to 22 h). (C) No polykaryons develop in the absence of trypsin. Bars = 50 um.

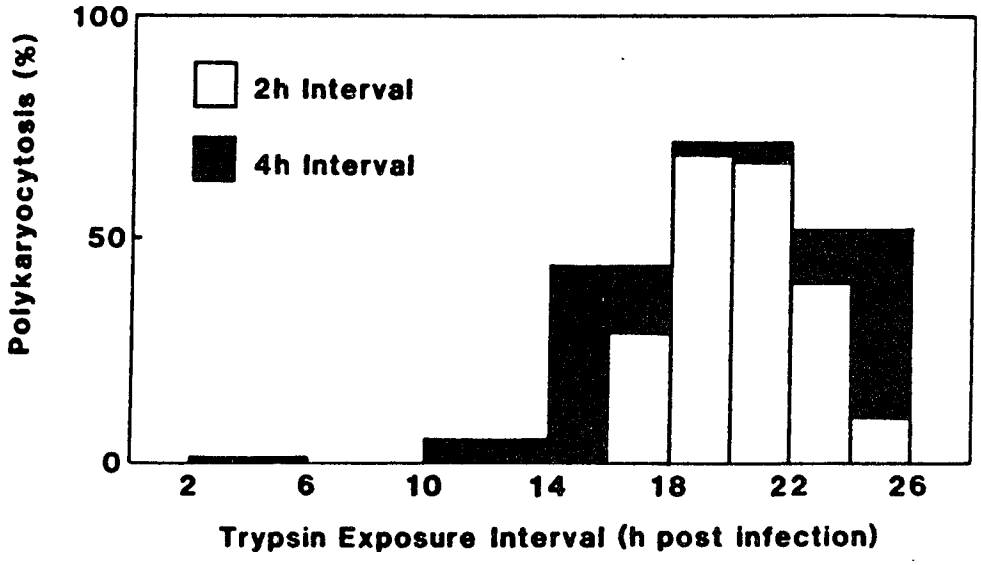

FIG. V.2. Trypsin activation of BCV-induced polykaryocytosis. Infected monolayers were exposed to trypsin for a single 2 or 4 h interval as indicated. Maximum polykaryocytosis occurred in cultures exposed to trypsin during the period from 18 to 22 h post infection.

V.C.3. Required pH level for fusion of infected cells. We then determined the pH level optimal for promotion of polykaryon formation. Infected cultures incubated for 19 h in the absence of trypsin were exposed for 2 h to trypsin-containing media at various pH levels. Trypsin treatment at pH 7.5 and 8.0 resulted in 20% and 39% polykaryocytosis respectively while treatments with media at lower pH levels produced no polykaryons. This result indicated that the fusion protein of BCV is not dependent on acidic conditions for activity.

V.C.4. Suppression of fusion by anti-BCV antibody. The trypsin requirement for BCV-induced cell fusion presented potential difficulties for our tests of fusion suppression by anti-viral antibody because of expected protein interactions. Fusion suppression was therefore examined by two different procedures. Exposure at 6 h post infection to medium containing both trypsin and antibody reduced polykaryon formation by 50%. Greater reduction occurred when infected monolayers were pretreated with the antibody. Pre-incubation with the antibody before trypsin treatment suppressed polykaryon formation by 81% over similar infected monolayers incubated with normal rabbit serum IgG.

V.D. DISCUSSION.

Many enveloped viruses are capable of inducing fusion of cultured cells. The fusion activity of alphaviruses, rhabdoviruses and myxoviruses strictly requires exposure of the virus-cell complex to

acidic conditions (37, 43, 158, 159). Cell fusion can, however, be induced at physiological pH by paramyxoviruses, either among cells infected at high multiplicity (fusion from without) or among infected cells (fusion from within) (56, 152). A specific glycoprotein component (F) of the paramyxovirus envelope is known to be involved in this membrane fusion activity. Fusion from without occurs when the active form of the F protein is expressed at the surface of paramyxovirus-infected cells. The precursor form of the F protein which is expressed at the surface of nonpermissive cells can be activated by treatment with an exogenous protease that cleaves the precursor at a specific site (119).

The suppression of polykaryon formation by anti-BCV treatments of infected cells indicates that coronaviral components were involved in cell fusion. Cells infected with the virus fused together in slightly basic environments. In this respect, the fusogenic potential of BCV resembles the paramyxovirus type of fusion activity. The trypsin requirement of the BCV fusion factor may involve a maturational cleavage of a coronaviral component analogous to the F protein of paramyxovirus. Although the fusion protein of BCV has not been identified, recent work revealed that trypsin treatment of infected cells or virions modifies several protein components of the BCV envelope (130, 161).

Trypsin exerted only a small effect on the yield of infectious virus in a single cycle of virus replication in BFS cells. The hemagglutination titer increased substantially after trypsin treatment. This effect probably resulted from a disaggregation of clumps of

noninfectious material because the infectious virus yield did not rise appreciably. Amplification of the virus infection apparently does not account for the required presence of trypsin for fusion activity. Trypsin modifications of BCV proteins may activate the viral fusion factor without producing a net change in the total number of infectious particles.

We identified a period of virus replication during which a 2 h trypsin treatment would produce polykaryons. This brief treatment was used to avoid possible fluctuations in pH that might occur during a prolonged treatment. Infected cultures at 18 to 22 h were most susceptible to the brief trypsin treatment. This period begins at the observed onset of fusion in cultures treated continuously with trypsin. The optimal time may be related to the appearance of a critical level of the BCV fusion proteins at the cell surface. Trypsin treatments that began at 22 or 24 h produced fewer polykaryons, possibly, because insufficient time was available for the fusing cells to coalesce and become visibly multinucleated.

Trypsin treatments during the time of maximal susceptiblity were effective only when media with pH levels of 7.5 or 8.0 were used. To provide excess proteolytic activity, trypsin was added at 1.0 ug per ml, a level 5 fold greater than that needed for cell fusion with continuous treatment at pH 7.8. The apparent ineffectiveness of treatments at acidic pH levels may be related to the optimal pH range for trypsin activity. Further investigation is necessary to determine the full range of pH levels at which the viral fusion protein is active. The results of the experiments described here demonstrate that

BCV-induced cell fusion may occur at alkaline pH levels. Therefore, the fusion protein of this virus is not strictly dependent on pH levels of 6 or less for activity.

The membrane fusion activity of another coronavirus, mouse hepatitis virus, also occurs at neutral and slightly alkaline pH levels (138). In this respect, the coronaviruses appear to resemble paramyxoviruses. Like these viruses, coronaviruses may be capable of penetrating the host cell by fusion with the plasma membrane during infectious entry.

CHAPTER VI: CHARACTERIZATION OF PLAQUES INDUCED BY BOVINE CORONAVIRUS REPLICATION IN HRT-18 CELLS

VI.A. INTRODUCTION.

Cytopathic interactions of bovine coronavirus with intestinal cells induce serious enteric disease in neonatal calves (33, 34, 54). These interactions have been studied in several cell lines (28, 135, 144, 148). Some field strains of BCV, which fail to replicate in other cells can be cultivated in HRT-18 cells, an intestinal cell line derived from an adenocarcinoma (145). A large percentage of the HRT-18 cells survive in the infected culture even when viral cytopathic expression is enhanced by the inclusion of trypsin in the culture medium (130). The surviving cells impart a characteristic turbidity to BCV-induced plaques.

This report describes scanning electron microscopic studies of HRT-18 cells resistant to the cytolytic effects of BCV. Apparent similarities between these cells and persistently infected HRT-18 cultures were explored as well.

VI.B. MATERIALS AND METHODS.

VI.B.1 Cells and virus. Monolayers of the human rectal tumor cell line HRT-18 (145) were maintained in Dulbecco modified Eagle medium (DMEM) buffered with 44 mM $NaHCO_3$ and supplemented with 5% fetal calf serum. Stock preparations of the Mebus strain L9 of BCV (121, 131) were propagated in HRT-18 cells. Virus stocks were generated from cells infected at a multiplicity of approximately 0.01 PFU per cell,

incubated for 4-5 days at 37°C in serum-free DMEM and harvested by freeze-thawing. Viral titers obtained in these preparations ranged from 10^6 to 10^7 PFU per ml.

VI.B.2. Plaque formation. Plaques were produced by cultivation of the virus in monolayers of HRT-18 cells grown in 6-well tissue culture dishes. The monolayers were incubated for 1 h at 37°C with dilute suspensions of the virus in DMEM. The virus-adsorbed monolayers were washed with DMEM and covered with an overlay consisting of DMEM with 0.6% agarose (Bethesda Research Laboratories) and 5 ug of trypsin (Difco Laboratories) per ml to enhance plaque formation (135). The plates were incubated for 2 to 4 d at 37°C in an atmosphere of 5% CO_2. After plaque development, the agarose overlay was removed from the cultures with a spatula. The monolayers were washed with PBS and fixed at 4°C for 30 min in 2% glutaraldehyde and 2% formaldehyde buffered with 0.1 M sodium cacodylate, pH 7.4.

VI.B.3. Hemadsorption by plaques. Cells in the plaques bearing viral hemagglutinin were identified by their ability to adsorb erythrocytes to the cell surface. The agarose was removed at 60 h post infection from monolayers containing trypsin-enhanced plaques. The monolayers were washed three times with 0.01 M $NaPO_4$, 0.14 M NaCl at pH 7.3 (PBS) to remove the residual agarose, covered with a suspension of 6 X 10^6 mouse erythrocytes per ml in PBS, and incubated for 20 min at 25°C to allow hemadsorption. The plaques were washed twice more with PBS to remove unbound erythrocytes and fixed at 4°C for 30 min in 2%

glutaraldehyde and 2% formaldehyde in 0.1 M sodium cacodylate buffer, pH 7.4.

VI.B.4. Processing for scanning electron microscopy. Monolayers fixed for scanning electron microscopy were washed in 0.1 M sodium cacodylate buffer pH 7.4 and gently debased from the plastic culture dishes with a cell scraper. Areas of interest were cut from the monolayers with razor blades into segments approximately 5 mm^2. The segments were incubated at 25^0C in sodium cacodylate buffered solutions (pH 7) of 1% osmium tetroxide for 30 min, 1% tannic acid for 15 min, and again in 1% osmium tetroxide for 15 min to deposit a conductive coating on the cell surface. After a final rinse in distilled water, the samples were dehydrated in an alcohol series, critical point dried from CO_2 in a critical point drying aparatus (Poloron Equipment), mounted with tape on aluminum stubs, and coated with an alloy of gold and palladium. The specimens were examined with a Cambridge S-150 scanning electron microscope.

VI.B.4. Establishment of persistently infected cultures. Monolayers of HRT-18 cells were grown in 25 cm^2 flasks and inoculated with BCV at a multiplicity of approximately 0.01 PFU per cell to establish persistent infections. The cultures were incubated at 37^0C for 6 to 12 days in serum-free medium. Trypsin (5 ug per ml) was added to the incubation medium of certain cultures to enhance the cytopathic expression of the virus during the establishment of persistence. Supernatant fluid containing released virus was harvested at weekly

intervals for plaque and hemadsorption assays and the cultures were passaged and covered with DMEM supplemented with 5% fetal calf serum.

VI.B.6. Indirect immunofluorescence. Viral antigens in cells were traced with fluorescent antibody. The infected monolayers were fixed for 10 min in 4% formaldehyde in PBS with 0.005% $CaCl_2$ and 0.11 M sucrose, permeabilized for 5 min with acetone at -20^{0}C, incubated with rabbit anti-BCV antibody, and reacted with goat anti-rabbit antibody conjugated to fluorescein isothiocyanate. The preparations were viewed with a Leitz fluorescent microscope using epifluorescence.

VI.C. RESULTS.

VI.C.1. Characteristics of viral plaques in HRT-18 cells. A scanning electron micrograph depicting the apical surface of an HRT-18 cell monolayer is illustrated in figure VI.1. The epitheliod appearance of the confluent monolayer resulted from the close associations between the polygonal cells. The apical surface of each cell was modified by a variable number of small filiform microvilli which were most numerous at the cell margins.

BCV-induced plaques at 3 days after plating in the presence of trypsin were round, 1 to 2 mm-in-diameter, and had sharp edges. Interior regions of the plaques were visibly turbid except at trypsin concentrations higher than 5 ug per ml. The plaque margins were defined by a peripheral area of extensive monolayer destruction that was revealed with the scanning electron microscope (FIG. VI.2). Many of the cells had detached from this marginal region leaving holes in the

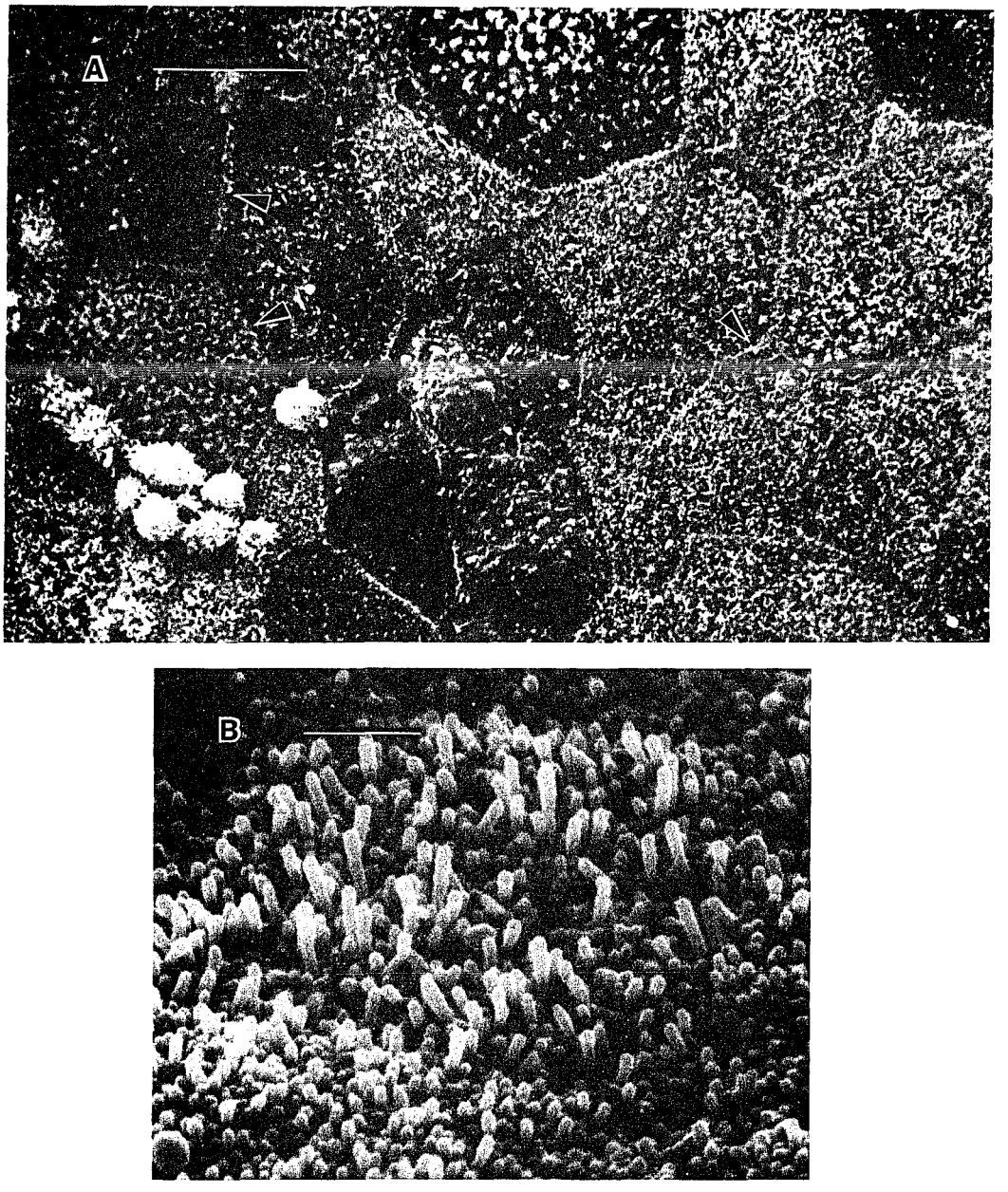

FIG. VI.1. Scanning electon micrographs of a control monolayer of uninfected HRT-18 cells. (A) Cell borders are denoted by arrowheads. Bar = 10 um. (B) Microvilli at apical cell surface are filiform. Bar = 1 um.

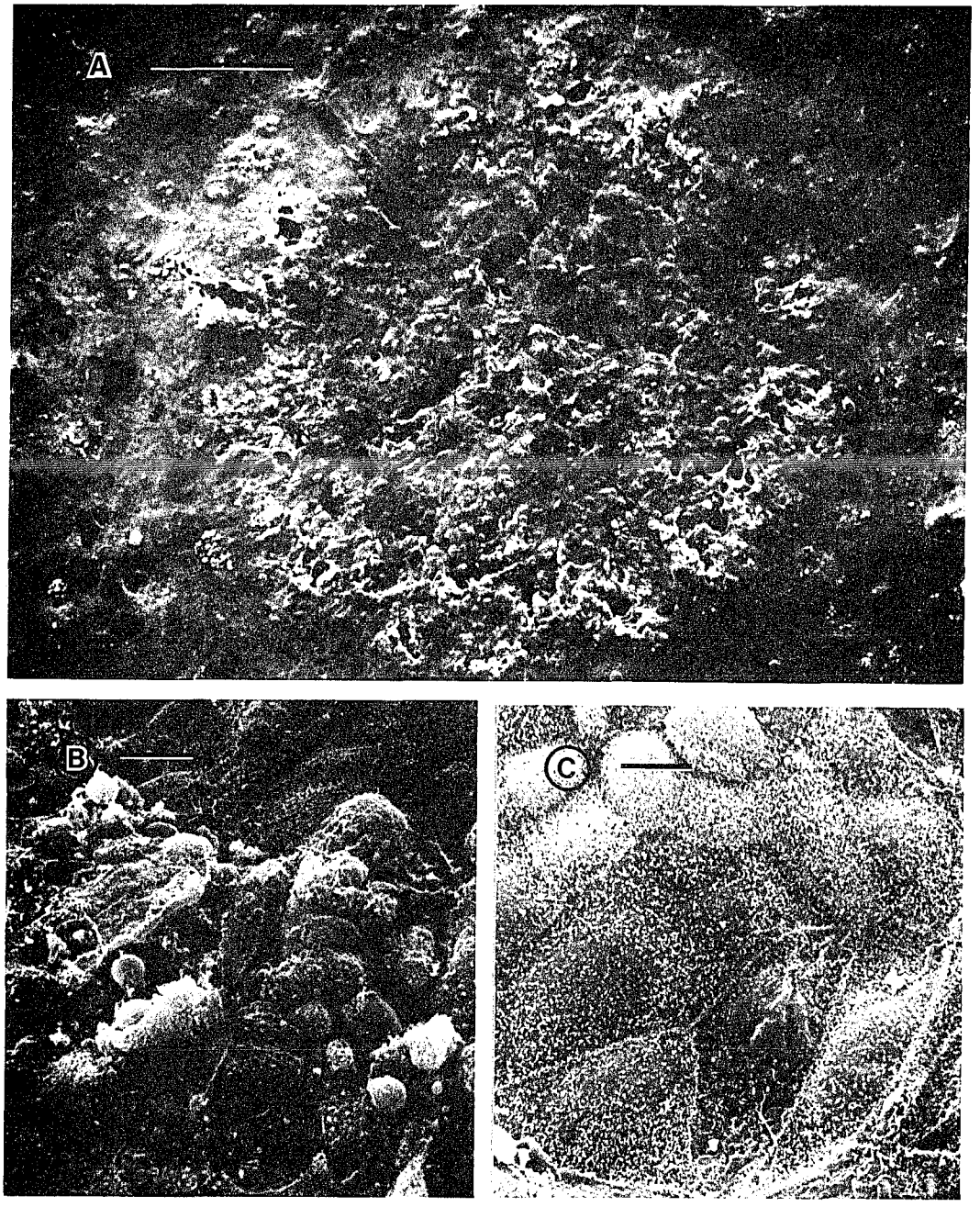

FIG. VI.2. Plaque induced by BCV replication for 60 h in HRT-18 monolayer. (A) Monolayer disruption is greatest at margin of entire plaque. Bar = 0.2 mm. (B) Depiction of cell damage at the plaque margin. Bar = 10 um. (C) A community of undamaged cells in plaque center. Bar = 10 um.

monolayer. The remaining cells frequently presented evidence of viral cytopathic expression consisting of cell rounding, plasma membrane damage, cytolysis and separation from adjoining cells. Monolayer damage was less prominent at interior areas of the plaques where unaffected cells predominated.

VI.C.2. Hemadsorption by plaques. Virus particles, 100 to 130 nm in size, where observed on the surfaces of HRT-18 cells in infected monolayers (FIG. VI.3). The abundance of virus particles varied widely from cell to cell. Cells in the interior regions of plaques that were apparently unaffected by the virus infection generally possessed few or no surface particles. We incubated plaques with erythrocytes to test for hemadsorption by these cells. Mouse erythrocytes were adsorbed to the microvilli of cells bearing surface virions (FIG. VI.4). The virions contributed to erythrocyte-cell binding by bridging the membrane surfaces. Hemadsorbing cells were most prominent near the plaque margin (FIG. VI.5A). This region of infected cells extended at least 100 um beyond the margin of the plaque as defined by cell structural damage. Damaged cells were also present at interior regions of the plaques but more than 90% of the cells were free of erythrocytes (FIG. VI.5B). The hemadsorbing cells frequently had signs of viral cytopathic effects but the cells which lacked viral hemagglutinin were structurally normal except for the some microvillous clustering which appeared to be a response to the agarose overlay. Areas of the monolayer at the plaque interior were less densely populated with cells.

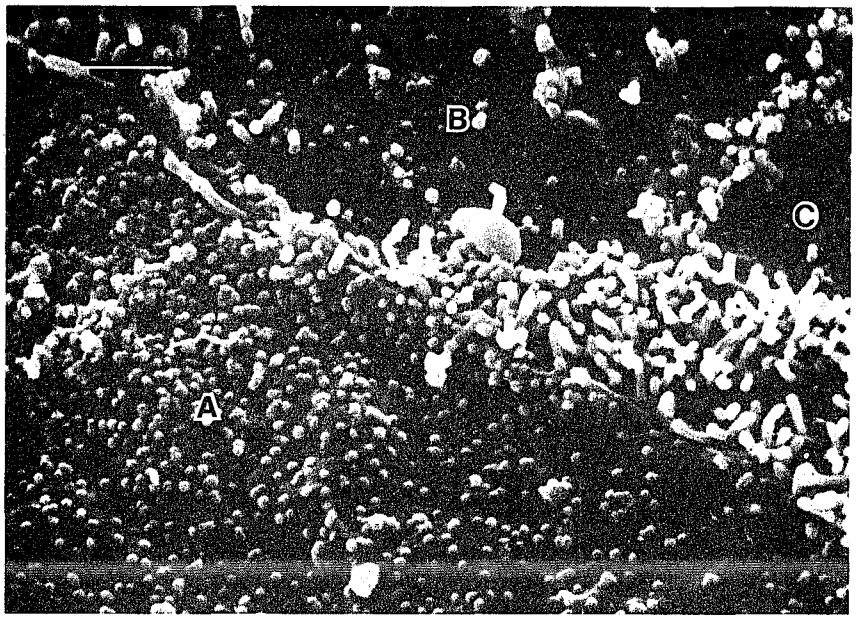

FIG. VI.3. Adsorption of virus particles to the cell surface. Virus particles (arrowheads) are abundant on cell (A) but less numerous on adjacent cells (B,C). Bar = 1 um.

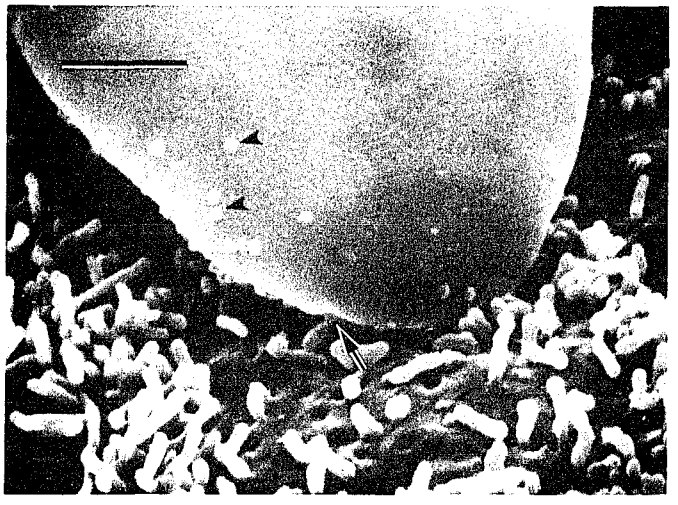

FIG. VI.4. Erythrocyte bound to surface of HRT-18 cell. Note virus particles (arrowheads) on erythrocyte, on cell surface and on microvillus linked to erythrocyte (arrow). Bar = 1 um.

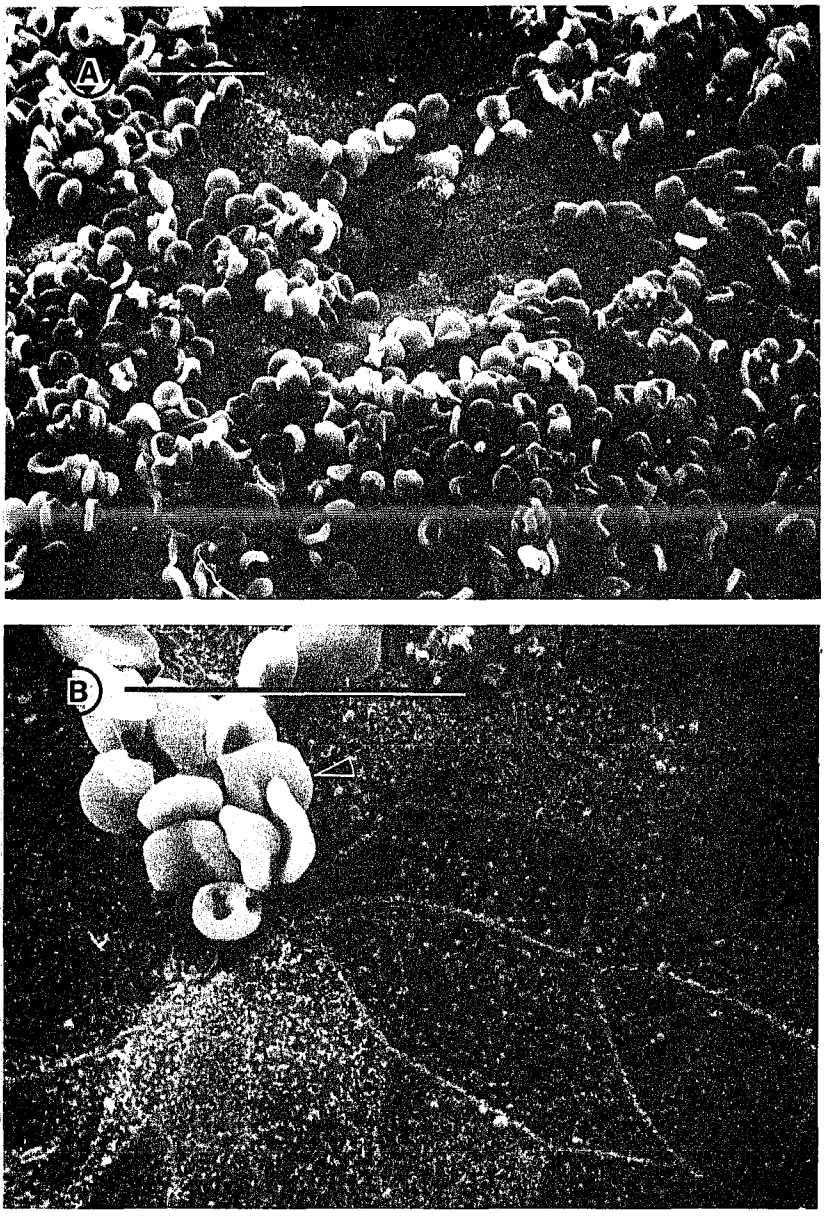

FIG. VI.5. Plaque incubated with erythrocytes. (A) Erythrocytes bind to many cells at plaque margin. (B) Central regions of the plaque contain few cells that have adsorbed erythrocytes (arrowhead). The structurally damaged cell is surrounded by normal cells that lack viral hemagglutinin. Bars = 20 um.

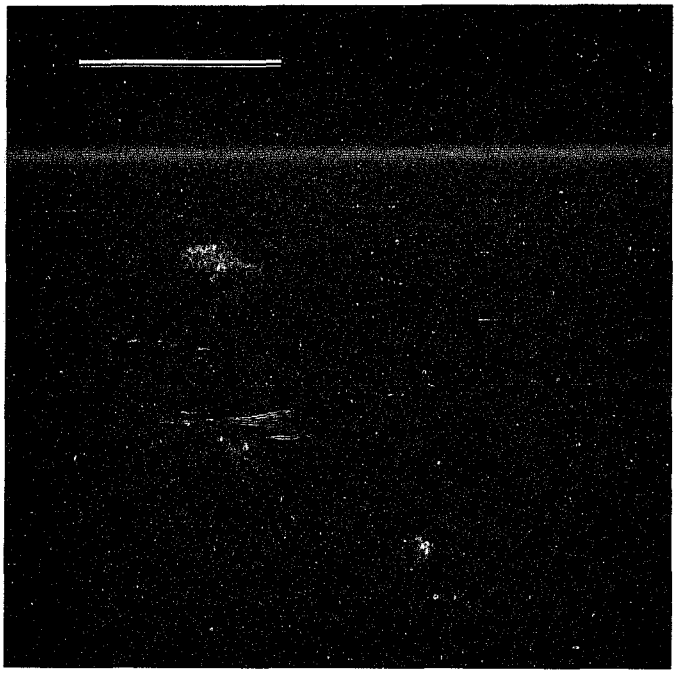

FIG. VI.6. Immunofluorescence of virus infected cells in an HRT-18 carrier culture at passage level 3.

VI.C.3. HRT-18 cultures persistently infected with BCV. We inoculated monolayers of HRT-18 cells with BCV to establish persistently infected cultures. Cytopathic expression of the virus consisted of cell rounding, monolayer vacuolization, and, in cultures incubated with trypsin, a limited amount of fusion. These effects were maximal at 4 to 5 d post infection but the damaged monolayers remained nearly confluent. Monolayers incubated with trypsin eventually detached from the plastic substrate.

Many cells survived the initial infection. They rapidly established confluent monolayers when the infected cultures were passaged and incubated with medium containing 5% serum to facilitate cell attachment and growth. The cell number increased at least 10 fold at each passage and viral cytopathic expression was not readily evident. These cultures carried the virus infection for 8 passages at which time the experiment was concluded. Immunofluorescence analysis revealed that only 10 to 15% of the cells in these carrier cultures contained viral antigens (FIG. VI.6). The hemagglutinating activity varied from 4 to 64 in samples of culture supernatants and the infectivity titers ranged from 7.0×10^5 to 7.2×10^6 PFU per ml.

VI.D. DISCUSSION.

Cells of the HRT-18 line were very closely associated in confluent monolayers. This association and the presence of filiform microvilli on the apical surface reflect the epithelial origin of the cell line. Scanning electron microscopy revealed a heterogenous

mixture of cells in the monolayer. Cell-to-cell diversity was apparent both in the number of microvilli at the apical surface and in the abundance of coronavirions which adsorbed to the plasmalemma in infected cultures. The abundance of surface-adsorbed coronavirions may relate to the concentration of cellular receptors for the virus. Both of these features could be a function of the cell cycle or they may be characteristic of stable subpopulations in the culture. The heterogeneity of the HRT-18 cell line was recently studied with cloned sublines which differ in their susceptibility to viral cytopathic expression (130).

The coronavirus multiplied in HRT-18 cells and, in the presence of trypsin, induced pronounced cytopathic changes in the monolayer. Plaques formed as the result of viral destruction of susceptible cells yet a residual turbidity remained. The outer margin of the plaque was defined by a peripheral zone of monolayer disruption. The central area was covered with a nearly confluent monolayer of structurally normal cells that lacked viral hemagglutinin. This plaque morphology may have developed by the following process: (i) A progession of infections which began with a single cell spread centrifugally to neighboring susceptible cells. These infected cells suffered the effects of viral cytopathic expression, lysed, and ultimately detached from the monolayer. (ii) Unaffected cells in the plaque interior maintainted confluence by a reorganization of their intercellular junctions while the lysed cells were released. Cell regrowth probably was not a factor in the maintenance of this monolayer because the overlay lacked serum to support an increase in cell number. (iii) Susceptible cells at the

periphery of the plaque were more recently infected. Monolayer disruption, therefore, was greatest at the peripheral zone of the plaque because these cells had not yet disintegrated or detached. This margin represented the advancing front of the spreading plaque.

Normal cells coexisted with a small number of infected cells at the plaque center in an association that was reminiscent of a persistent infection. We found that the virus persisted in HRT-18 cultures. Viral antigens were produced by a minority of the cells in carrier cultures and progeny virus was released consistently for at least 8 passages. Cell growth was affected little by the infection and cytopathic expression of the virus was minimal when the culture medium was supplemented with serum. These persistently infected cultures were easily established and appeared to be stable.

Possible mechanisms involved in the establishment of persistent coronaviral infections include conditional interference by emerging temperature-sensitive or poorly growing mutants (6), the development of defective interfering virus (84), and the production of interferon (5). Cell cycle-dependent variations in the expression of cellular receptors or organelles may place a temporal limit on host susceptibility to BCV. This could allow continued HRT-18 cell growth and development of daughter cells in the culture. We feel that cellular determinants are probably an important factor in BCV persistence in these cultures because of the heterogeneity of HRT-18 cells and the presence of subpopulations with intrinsic resistance to the virus. Such cells have been found to be involved in the establishment of a persistent murine coronavirus infection on a subline of L cells (99).

CHAPTER VII: SUMMARY AND PERSPECTIVES OF INVESTIGATIONS

VII.A. SUMMARY OF FINDINGS.

The aim of our investigation was to analyze the morphogenetic aspects of the membrane-associated stages of BCV replication. We used morphological and physiological methods to analyze the entry of BCV into HRT-18 cells. Immunoelectron microscopy revealed that many of the virus particles were endocytosed while other virions fused with the cell surface. The endosomal environment apparently failed to trigger virus fusion along intracellular membranes and these particles accumulated in secondary lysosomes. Endocytosis of virus particles apparently represented an abortive infection. Our analyses of the effects of lysosomotropic weak bases on BCV replication indicated that an acidic compartment is not involved in BCV entry. Ammonium chloride treatment, which results in a neutralization of the normally acidic endosomal environment (93), was not inhibitory for the first hour of infection. Suppression of the infection by ammonium chloride would have supported the endocytic pathway for infectious entry by BCV. We concluded that infectious entry by BCV does not involve the endocytic route thus implying that the cells were infected by direct fusion of the virion with the plasmalemma.

The viral fusion factor was characterized by analyzing the conditions required for BCV-induced polykaryocytosis. Virus infected cells formed polykaryons in neutral to slightly basic media containing trypsin. This finding is consistent with the hypothesis that BCV

enters its host cell by direct fusion with the plasmalemma under normal physiological conditions.

Simultaneous fusion of large numbers of virions with the surface membranes of adjacent cells may induce polykaryon formation from without. Cell fusion alternatively may result from the action of viral components expressed in the plasma membrane. We used immunoelectron microscopy to demonstrate that BCV antigens are expressed de novo in the plasma membrane of infected cells despite the intracellular mode of coronaviral maturation. These antigens probably included the viral fusion factor because the structures were localized by the same antibody that causes a partial suppression of polykaryon formation.

Cytopathic expression of BCV replication results in plaques in monolayers of HRT-18 cells. Scanning electon microscopy revealed that the characteristic turbidity of these plaques is caused by the presence in the plaque interior of structurally normal cells that lack viral hemagglutinin. These cells survived in the plaque interior while the infected cells lysed.

VII.B. CORONAVIRUS ENTRY.

The observation that many BCV particles were endocytosed by the cell was not an unexpected finding. Endocytosis is a normal cellular process for internalizing extracellular material including inactive virus particles. Unfavorable ratios of physical virus particles to infectious particles persistently burden morphological and biochemical studies of the initial events of virus infection (32). The endocytosis of BCV probably represents cellular scavenging of

"non-infectious" particles. Since we were unable to find clear evidence of fusion along intracellular endosomal membranes, we did not find endocytosis relevant to BCV entry. An immunolocalization approach similar to ours was employed by Nemerow and Cooper (101) to study entry of Epstein-Barr virus into L cells. They clearly documented sites of viral deenvelopment in intracellular vesicles with the immunogold technique. Fusion of this herpesvirus with the surface membrane was not observed.

We found that ammonium chloride was not an efficient inhibitor of the early stages of BCV replication but this result appears to conflict with studies of other coronaviruses. Recent investigations of MHV replication cited evidence of ammonium chloride suppression to support the conclusion that this coronavirus enters its host cell by the endocytic route (73, 98, 146). Krzystniak and Dupuy (73), for example, described an inhibitory effect of ammonium chloride on MHV infection but their experiments involved very low multiplicities of infection (1×10^{-5} to 2×10^{-4} PFU per cell). The authors reported that the inhibitory effect of ammonium chloride was eliminated when addition of the base was delayed until 3 h post infection.

This lack of inhibition with delayed treatment is difficult to understand if one considers that the low multiplicity of infection would allow multiple cycles of infections to amplify even small effects of the base. Ammonium chloride inhibition of MHV infection was also reported by Tooze and Tooze (146) but this effect was seen at higher drug concentrations (30 mM) which may cause nonspecific cytotoxicity. The apparent antiviral activity of lysosomotrophic agents can result

from effects other than a block in the transport of the virus genome into the cell cytoplasm (13).

Mizzen, et al. (98) discovered that ammonium chloride delays rather than inhibits MHV infection and does not affect the ultimate yield of progeny virus. They concluded that the primary effect of the base was to attenuate post fusion events by some undefined action on MHV uncoating during the eclipse phase. Our experiments, in comparison to the studies of MHV entry, involved cultures that were infected at high multiplicity to produce synchronous replication. We harvested the cultures at a time when virus yield would have included BCV production that might have been delayed by treatment with the base.

These deviations in experimental design and interpretation of the results could explain the apparent conflict about the effect of ammonium chloride on coronavirus entry. MHV may in fact differ from BCV in its response to the lysosomotroph but it is difficult to comprehend that different coronaviruses enter the host cell by alternative routes. It has been suggested that a number of viruses are capable of entering cells by direct fusion as well as the endocytic route. For example, electron microscopic studies revealed that the envelope of vaccinia virus integrated with the L cell plasma membrane (32) with endocytosis occurring as a later event and possibly involving only incomplete particles. Coronaviruses can, perhaps, infect host cells by either route but certainly one of the alternatives is the predominant mode of entry for a particular virus:host combination.

Virus-cell fusion during entry and virus-induced cell fusion appear to be based on the same principle (68). A virus dependent on

the endocytic route of entry for infection would therefore be expected to have fusion proteins active at the acidic environment encountered in the endosome. Cell fusion induced by BCV decidedly was not dependent on low pH conditions for activity. This phenomenon supports the hypothesis that BCV can infect cells by direct entry. The BFS line was used for this test because BCV infection of these cells results in countable polykaryons. Quantitation of the extent of fusion was not possible with the HRT-18 cell line. Large globular masses (presumably products of cell fusion) are formed in infected HRT-18 cultures but the number of nuclei per globule is not readily determined. The analysis of BCV entry should be extended by a study of the entry of the virus into the BFS host cell. Cell-to-cell fusion appears to occur more readily in these cells so fusion of virions with the plasma membrane may be more efficient than with HRT-18 cells.

VII.C. CELLULAR EXPRESSION OF CORONAVIRAL ANTIGENS.

Control of virus spread in vivo may involve immune recognition of virus specific antigens on the cell surface. The infected cells may then be removed prior to the release of progeny virus. Immune recognition and attack would be expected to remove BCV-infected enterocytes more efficiently if the viral antigens were expressed in basolateral aspects of the plasma membrane as well. Infected HRT-18 cells were found to express BCV antigens in the apical plasma membrane, but we were unable to determine if the antigens were also present at basolateral domains.

The assembly of many enveloped viruses is assymetrical in polarized epithelial cells because the viral envelope glycoproteins are segregated to either the apical or the basolateral membrane domains (113). Alonso-Caplen et al. (2) reported that assembly of the avian coronavirus IBV is susceptible to inhibition by monensin -- an ionphore that selectively blocks transport of vesicular stomatitis virus glycoproteins to the basolateral membrane domain (1). Other than this indication of the involvement of directed transport to the basolateral membrane, the polarity of coronavirus release has not been determined. An important extension of our work would be an analysis of antigen expression in the basolateral and apical plasma membrane of infected enterocytes of calves inoculated with BCV.

A polyclonal mixture of antibodies has practical advantages for immunoelectron microscopy but the rabbit antiserum was unable to distinguish among the various antigenic components of BCV. Further analysis of viral antigen expression in BCV infected cells should involve affinity purified or monoclonal antibody probes that can detect individual viral proteins. These investigations could determine if particular proteins are expressed at restricted locations in the cell. Our attempts to localize intracellular BCV antigens with post-embedment immunolabeling techniques were unsuccessful. An alternative technique--pre-embedment localization in cells permeabilized with saponin--may be more successful for detecting the intracellular locations of BCV proteins.

VII.D. TRYPSIN ENHANCEMENT OF BCV PLAQUES.

Turbid plaques were formed in the presence of trypsin by BCV infection of HRT-18 cell monolayers. The characteristic turbidity resulted from the survival of structurally normal cells that were hemagglutinin negative. These cells were found in a sub-confluent monolayer that apparently formed from a reorganization of intracellular junctions after infected cells disintegrated. This reorganization may be facilitated by trypsin action in weakening the intracellular junctions. An effect on the mobility of HRT-18 cells could augment other mechanisms that may be responsible for trypsin enhancement of plaque formation such as activation of a viral fusion factor (130, 135).

VII.E. SIGNIFICANCE

BCV-induced enteritis in calves results primarily from cytocidal effects of virus replication in susceptible enterocytes. Membrane-associated events of BCV replication are important stages of the infection. These events are potential virulence factors because interactions between the virus and cellular membranes contribute to cell killing in many virus infections (68). An improved understanding of these events may, therefore, lead to practical benefits in prevention and control of coronaviral enteritis. These investigations are also significant as contributions to a basic understanding of viral and cellular interactions.

CHAPTER VIII: BIBLIOGRAPHY

1. Alonso, F.V., and R.W. Compans. 1981. Differential effect of monensin on enveloped viruses that form at distinct plasma membrane domains. J. Cell Biol. 89:700-705.

2. Alonso-Caplen, F.V., Y. Matsuoka, G.E. Wilcox, and R.W. Compans. 1983. Replication and morphogenesis of avian coronavirus in VERO cells and their inhibition by monensin. Virus Res. 1:153-167.

3. Andersen, K.B., and B.A. Nexo. 1983. Entry of murine retrovirus into mouse fibroblasts. Virology 125:85-98.

4. Appleyard, G., and M. Tisdale. 1985. Inhibition of the growth of human coronavirus 229E by leupeptin. J. Gen. Virol. 66:363-366.

5. Bang. F.B. 1982. The use of a genetically incompatible combination of host and virus (MHV) for the study of mechanisms of host resistance. Adv. Exp. Med. Biol. 142: 359-374.

6. Baybutt, H.N., H. Wege, M.J. Carter, and V. ter Meulen. 1984. Adaptation of coronavirus JHM to persistent infection of murine sac(-) cells. J. Gen. Virol. 65:915-924.

7. Bingham, R.W., and J.D. Almeida. 1977. Studies on the structure of a coronavirus-avian infectious bronchitis virus. J. Gen. Virol. 36:495-502.

8. Binns, M.M., M.E.G. Boursnell, D. Cavanaugh, D.J.C. Pappin, and T.D.K. Brown. 1985. Cloning and sequencing of the gene encoding the spike protein of the coronavirus IBV. J. Gen. Virol. 66:719-726.

9. Boursnell, M. E. G., T. D. K. Brown, I. J. Foulds, P. F. Green, F. M. Tomley, and M. M. Binns. 1987. Completion of the sequence of the genome of the coronavirus avian infectious bronchitis virus. J. Gen. Virol. 68:57-77.

10. Bridger, J.C., E.O. Caul, and S.I. Egglestone. 1978. Replication of an enteric bovine coronavirus in intestinal organ culture. Arch. Virol. 57:43-51.

11. Buchmeier, M.J., H.A. Lewicki, P.J. Talbot, and R.L. Knobler. 1984. Murine hepatitis virus-4 (strain JHM) induced neurologic disease is modulated in vivo by monoclonal antybody. Virology 132:261-270.

12. Callebaut, P.E., and M. B. Pensaert. 1980. Characterization and isolation of structural polypeptides in haemagglutinating encephalomyelitis virus. J. Gen. Virol.48:193-204.

13. Cassell, S., J. Edwards, and D.T. Brown. 1984. Effects of lysosomotropic weak bases on infectio ı of BHK-12 cells by Sindbis virus. J. Virol. 52:857-864.

14. Caul, E.O., C.R. Ashley, M. Ferguson, and S.I. Egglestone. 1979. Preliminary studies on the isolation of coronavirus 229E nucleocapsids. FEMS Microbiol. Let. 5:101-105.

15. Cavanagh, D. 1983. Coronavirus IBV glycopolypeptides: size of their polypeptide moieties and nature of their oligosaccharides. J. Gen. Virol. 64:1187-1191.

16. Cavanagh, D. 1983. Coronavirus IBV: further evidence that the surface projections are associated with two glycopolypeptides. J. Gen. Virol. 64:1787-1791.

17. Cavanagh, D. 1983. Coronavirus IBV: structural characterization of the spike protein. J. Gen. Virol. 64:2577-2583.

18. Chasey, D., and D. J. Alexander. 1976. Morphogenesis of avian infectious bronchitis virus in primary chick kidney cells. Arch. Virol. 52:101-111.

19. Choppin, P.W., and A. Scheid. 1980. The role of viral glycoproteins in adsorption, penetration, and pathogenicity of viruses. Rev. Infect. Dis. 2:40-61.

20. Collins, A.R., R.L. Knobler, H. Powell, and M.J. Buchmeier. 1982. Monoclonal Antibodies to murine hepatitis virus-4 (Strain JHM) define the viral glycoprotein responsible for attachment and cell-cell fusion. Virology 119:358-371.

20a. Collins, J.K., C.A. Riegel, J.D. Olson, and A. Fountain. 1987. Shedding of enteric coronavirus in adult cattle. Am. J. Vet. Res. 48:361-365, 1987.

21. Collins, M.S., and D.J. Alexander. 1980. Avian infectious bronchitis virus structural polypeptides: effect of different conditions of disruption and comparison of different strains and isolates. Arch. Virol. 63:239-251.

22. Corbo, L.J., and C.H. Cunningham. 1959. Hemagglutination by trypsin-modified infectious bronchitis virus. Am. J. Vet. Res. 20:876-883.

23. Crouch, C.F., H.B. Ohmann, T.C. Watts, and L.A. Babiuk. 1985. Chronic shedding of bovine enteric coronavirus antigen-antibody complexes by clinically normal cows. J. Gen. Virol. 66:1489-1500.

24. Dalziel, R.G., P.W. Lampert, P.J. Talbot, and M.J. Buchmeier. 1986. Site specific alteration of murine hepatitis virus type-4

(MHV-4) peplomer glycoprotein E2 results in reduced neurovirulence. J. Virol. 59:463-471.

25. David-Ferreira, J.F., and R.A. Manaker. 1965. An electron microscope study of the development of a mouse hepatitis virus in tissue culture cells. J. Cell Biol. 24:57-65.

26. Davies, H., and M.R. Macnaughton. 1979. Comparison of the morphology of three coronaviruses. Arch. Virol. 59:25-33.

27. De Groot, R.J., R.J. Ter Haar, M.C. Horzinek, and B.A.M. van der Zeijst. 1987. Intracellular RNAs of the feline infectious peritonitis coronavirus strain 79-1146. J. Gen. Virol. 68:995-1002.

28. Dea, S., R.S. Roy, and M.E. Begin. 1980. Bovine coronavirus isolation and cultivation in continuous cell lines. Am. J. Vet. Res. 41:30-38.

29. Denison, M., and S. Perlman. 1987. Identification of putative polymerase gene product in cells infected with murine coronavirus A59. Virology 157:565-568.

30. Dennis, D.E., and D.A. Brian. 1982. RNA-dependent RNA polymerase activity in coronavirus-infected cells. J. Virol. 42:153-164.

31. Deregt, D., M. Sabara, and L.A. Babiuk. 1987. Structural proteins of bovine coronavirus and their intracellular processing. J. Gen. Virol. 68:2863-2877.

32. Dimmock, N.J. 1982. Initial stages in infection with animal virus. J. Gen. Virol. 59:1-22.

33. Doughri, A.M., and J. Storz. 1977. Light and ultrastructural pathological changes in intestinal coronavirus infection of newborn calves. Zbl. Vet. Med. B. 24:367-385.

34. Doughri, A.M., J. Storz, I. Hajer, and H.S. Fernando. 1976. Morphology and morphogenesis of a coronavirus infecting intestinal epithelial cells of newborn calves. Exp. Mol. Pathol. 25:355-370.

35. Dubois-Dalcq, M.E., E.W. Doller, M.V. Haspel, and K.V. Holmes. 1982. Cell tropism and expression of mouse hepatitis viruses (MHV) in mouse spinal cord cultures. Virology 119:317-331.

36. Ducatelle, R., and J. Hoorens. 1984. Significance of lysosomes in the morphogenesis of coronaviruses. Arch. Virol. 79:1-12.

37. Edwards, J., and D.T. Brown. 1986. Sindbis virus-mediated cell fusion from without is a two-step event. J. Gen. Virol. 67:377-380.

38. Falke, D., A. Knoblich, and S. Muller. 1985. Fusion from without induced by herpes simplex virus type 1. Intervirology 24:211-219.

39. Fleming, J.O., M.D. Trousdale, F.A K. El-Zaatari, S.A. Stohlman, and L. P. Weiner. 1986. Pathogenicity of antigenic variants of murine coronavirus JHM selected with monoclonal antibodies. J. Virol. 58:869-875.

40. Forgac, M., L. Cantley, B. Wiedenmann, L. Altstiel, and D. Branton. 1983. Clathrin-coated vesicles contain an ATP-dependent proton pump. Proc. Natl. Acad. Sci. U.S.A. 80:1300-1303.

41. Frana, M.F., J.N. Behnke, L.S. Sturman, and K.V. Holmes. 1985. Proteolytic cleavage of the E2 glycoprotein of murine coronavirus. Host-dependent differences in proteolytic cleavage and cell fusion. J. Virol. 56:912-920.

42. Garwes, D.J., D.H. Pocock, and B.V. Pike. 1976. Isolation of subviral components from transmissible gastroenteritis virus. J. Gen. Virol. 32:283-294.

43. Gonzalez-Scarano, F., N. Pobjecky, and N. Nathanson. 1984. La Crosse bunyavirus can mediate pH-dependent fusion from without. Virology 132:222-225.

44. Graves, M.C., S.M. Silver, and P.W. Choppin. 1978. Measles virus polypeptide synthesis in infected cells. Virology 86:254-263.

45. Greig, A.S., C.M. Johnson, and A.M.P. Bouillant. 1971. Encephalitis of swine caused by a haemagglutinating virus. VI. Morphology of the virus. Res. Vet. Sci. 12:305-307.

46. Greig, A.S., D. Mitchell, A.H. Corner, G.L. Bannister, E.B. Meads, and R.J. Julian. 1962. A hemagglutinating virus producing encephalomyelitis in baby pigs. Can. J. Comp. Med. 26:49-56.

47. Helenius, A., J. Kartenbeck, K. Simons, and E. Fries. 1980. On the entry of Semliki forest virus into BHK-21 cells. J. Cell Biol. 84:404-420.

48. Helenius, A., M. Marsh, and J. White. 1982. Inhibition of Semliki forest virus penetration by lysosomotropic weak bases. J. Gen. Virol. 58:47-61.

49. Herndon, R.M., D.E. Griffin, U. McCormick, and L.P. Weiner. 1975. Mouse hepatitis virus-induced recurrent demyelination. Arch. Neurol. 32:32-35.

50. Holmes, K.V. 1985. Replication of coronaviruses, p. 1331-1343. In B.N. Fields, D.M. Knipe, R.N. Chanock, J. Melnick, B. Roizman, and R. Shope (ed.), Virology. Raven Press, New York.

51. Holmes, K.V., and J.N. Behnke. 1982. Evolution of a coronavirus during persistent infection in vitro. Adv. Exp. Med. Biol. 142:287-299.

52. Holmes, K.V., E.W. Doller, and J.N. Behnke. 1982. Analysis of the functions of coronavirus glycoproteins by differential inhibition of synthesis with tunicamycin. Adv. Exp. Med. Biol. 142:133-142.

53. Holmes, K.V., E.W. Doller, and L.S. Sturman. 1981. Tunicamycin resistant glycosylation of a coronavirus glycoprotein: Demonstration of a novel type of viral glycoprotein. Virology 115:334-344.

54. House, J.A. 1978. Economic impact of rotavirus and other neonatal disease agents of animals. J. Am. Vet Med. Assoc. 173:573-76.

55. Hsu, M-C., A. Scheid, and P.W. Choppin. 1983. Fusion of Sendai virus with liposomes: dependence on the viral fusion protein (F) and the lipid composition of liposomes. Virology 126:361-369.

56. Hsu, M.-C., A. Scheid, and P.W. Choppin. 1982. Enhancement of membrane fusion activity of Sendai virus by exposure of the virus to basic pH is correlated with a conformational change in the fusion protein. Proc. Nat. Acad. Sci. USA 79:5862-5866.

57. Huang, R.T.C., R. Rott, and H.-D. Klenk. 1981. Influenza viruses cause hemolysis and fusion of cells. Virology 110:243-247.

58. Jacobs, L., B.A.M. van der Zeijst, and M.C. Horzinek. 1986. Characterization and translation of transmissible gastroenteritis virus mRNAs. J. Virol. 57:1010-1015.

59. Kaye, H. S., and W. R. Dowdle. 1969. Some characteristics of hemagglutination of certain strains of "Avian bronchitis virus-like" viruses (coronavirus) similar to 229E virus, with some epidemiological observations. J. Infect. Dis. 120:576-581.

59a. Keck, J.G., B.G. Hogue, D.A. Grian, and M.M.C. Lai. 1988. Temporal regulation of bovine coronavirus RNA synthesis. Vir. Res. 9:343-356.

60. Kennedy D.A., and C.M. Johnson-Lussenburg. 1975/76. Isolation and morphology of the internal component of human coronavirus, strain 229E. Intervirology 6:197-206.

61. Kielian, M. C., S. Keranen, L. Kaariainen, and A. Helenius. 1984. Membrane fusion mutants of Semliki forest virus. J. Cell Biol. 98:139-145.

62. King, B., and D.A. Brian. 1982. Bovine coronavirus structural proteins. J. Virol. 42:700-707.

63. King, B., B.J. Potts, and D.A. Brian. 1985. Bovine coronavirus hemagglutinin protein. Virus Res. 2:53-59.

64. Klenk, H.-D., and R. Rott. 1980. Cotranslational and postranslational processing of viral glycoproteins. Curr. Top. Microbiol. Immunol. 90:19-25.

65. Knobler, R.L., J.V. Haspel, and M.B.A. Oldstone. 1981. Mouse hepatitis virus type 4 (JHM strain)-induced fatal central nervous system disease. I. Genetic control and the murine neuron as the susceptible site of disease. J. Exp. Med. 153:828-843.

66. Knobler, R.L., P.W. Lampert, and M.B.A. Oldstone. 1982. Virus persistence and recurring demyelination produced by a temperature-sensitive mutant of MHV-4. Nature 298:279-280.

67. Koga, M.H. Wege, and V. ter Meulen. 1984. Sequence of murine coronavirus JHM induced neuropathological changes in rats. Neuropathol. Appl. Neurobiol. 10:173-184.

68. Kohn, A. 1985. Membrane effects of cytopathogenic viruses. Prog. Med. Virol. 31:109-167.

69. Kohn, A. 1965. Polykaryocytosis induced by Newcastle desease virus in monolayers of animal cells. Virology 26:228-245.

70. Kojima, A., H. Takada, and A. Okaniwa. 1986. Multiplication of canine coronavirus in CRFK cells. Jpn. J. Vet. Sci. 48:1063-1070.

71. Koolen, M.J.M., S. Love, W. Wouda, J. Calafat, M.C. Horzinek, and B.A.M. van der Zeijst. 1987. Induction of demyelination by a temperature-sensitive mutant of the coronavirus MHV-A59 is associated with restriction of viral replication in the brain. J. Gen. Virol. 68:703-714.

72. Krzystniak, K., and J.M. Dupuy. 1981. Early interaction between mouse hepatitis virus 3 and cells. J. Gen. Virol. 57:53-61.

73. Krzystniak, K., and J.M. Dupuy. 1984. Entry of mouse hepatitis virus 3 into cells. J. Gen. Virol. 65:227-231.

74. Lai, M.M.C., P.R. Brayton, R.C. Armen, C.D. Patton, and S.A. Stohlman. 1981. Mouse hepatitis virus A59 messenger RNA structure and genetic localization of the sequence divergence from the hepatropic strain MHV3. J. Virol. 39:823-834.

75. Lai, M.M.C. 1986. Coronavirus leader-RNA-primed transcription: an alternative mechanism to RNA splicing. Bioessays 5:257-260.

76. Lai, M.M.C., C.D. Patton, and S.A. Stohlman. 1982. Replication of

mouse hepatitis virus: negative-stranded RNA and replicative form RNA are of genome length. J. Virol. 44:487-492.

77. Lamontagne, L., P. Marois, E. DiFranco, and R. Assaf. 1981. Inner structures of some coronaviruses. Can. J. Comp. Med. 45:177-181.

78. Lapps, W., B.G. Hogue, and D.A. Brian. 1987. Sequence analysis of the bovine coronavirus nucleocapsid and matrix protein genes. Virology 157:47-57.

79. Lenard, J., and K.D. Miller. 1982. Uncoating of enveloped viruses. Cell 28:5-6.

80. Lomniczi, B. 1977. Biological properties of avian coronavirus RNA. J. Gen Virol. 36:531-533.

81. Macnaughton, M.R., and M.H. Madge. 1978. The genome of human coronavirus strain 229E. J. Gen. Virol. 30:497-504.

82. Macnaughton, M.R. 1980. The polypeptides of human and mouse coronaviruses. Arch. Virol. 63:75-80.

83. Mahy, B.W.J., S. Siddell, H. Wege, and V. ter Meulen. 1983. RNA-dependent RNA polymerase activity in murine coronavirus-infected cells. J. Gen. Virol. 64:103-111.

84. Makino, S., F. Taguchi, and D. Fujiwara. 1984. Defective interfering particles of murine hepatitis virus. Virology 133:9-17.

85. Makino, S., S.A. Stohlman and M.M.C. Lai. 1986. Leader sequences of murine coronavirus mRNAs can be freely reassorted: evidence for the role of free leader RNA in transcription. Proc. Natl. Acad. Sci. U.S.A. 83:4204-4208.

86. Mallucci, L. 1966. Effect of chloroquine on lysosomes and on growth of mouse hepatitis virus (MHV-3). Virology 28:355-362.

87. Mann, E., J. Edwards, and D.T. Brown. 1983. Polycaryocyte formation mediated by Sindbis virus glycoproteins. J. Virol. 45:1083-1089.

88. Marsh, M., E. Bolzau, and A. Helenius. 1983. Penetration of Semliki forest virus from acidic prelysosomal vacuoles. Cell 32:931-940.

89. Marsh, M., and A. Helenius. 1980. Adsorptive endocytosis of Semliki Forest virus. J. Mol. Biol. 142:439-454.

90. Marsh, M., K. Matlin, K. Simons, H. Reggio, J. White, J. Kartenbeck, and A. Helenius. 1982. Are lysosomes a site of

enveloped-virus penetration? Cold Springs Harbor Symp. Quant. Biol. 46:835-843.

91. Massalski, A., M. Coulter-Mackie, R.L. Knobler, M.J. Buchmeier, and S. Dales. 1982. In vivo and in vitro models of demyelinating diseases. V. Comparison of the assembly of mouse hepatitis virus, strain JHM, in two murine cell lines. Intervirology 18:135-146.

92. Matlin, K. S., J. Reggio, A. Helenius, and K. Simons. 1981. Entry pathway of influenza virus in a canine kidney cell line. J. Cell Biol. 91:601-613.

93. Maxfield, F.R. 1982. Weak bases and ionophores rapidly and reversibly raise the pH of endocytic vesicles in cultured mouse fibroblasts. J. Cell Biol. 95:676-681.

94. McIntosh, K. 1985. Coronaviruses, p. 1323-1330. In B.N. Fields, D.M. Knipe, R.N. Chanock, J. Melnick, B. Roizman, and R. Shope (ed.), Virology. Raven Press, New York.

95. Mebus, C.A., M.B. Rhodes, and M.J. Twiehaus. 1973. Neonatal calf diarrhea: propagation, attenuation, and characteristics of a coronavirus-like agent. Am. J. Vet. Res. 3:145-150.

96. Mebus, C.A., M.B. Rhodes, and N.R. Underdahl. 1978. Neonatal calf diarrhea caused by a virus that induces villous epithelial cell syncytia. Am. J. Vet. Res. 39:1223-1228.

97. Mengeling, W.L., A.D. Boothe, and A.E. Ritchie. 1972. Characteristics of a coronavirus (strain 67N) of pigs. Am. J. Vet. Res. 33:297-308.

98. Mizzen, L., A. Hilton, S. Cheley, and R. Anderson. 1985. Attenuation of murine coronavirus infection by ammonium chloride. Virology 142:378-388.

99. Mizzen, L., S. Cheley, M. Rao, R. Wolf, and R. Anderson. 1983. Fusion resistance and decreased infectability as major host determinants of coronavirus persistence. Virology 128:407-417.

100. Mollenhauer, H.H. 1964. Plastic embedding mixtures for use in electron microscopy. Stain Technol. 39:111-114.

101. Nemerow, G.R., and N.R. Cooper. 1984. Early events in the infection of human B lymphocytes by Epstein-Barr virus: the internalization process. Virology 132:186-198.

102. Niemann, H., B. Boschek, D. Evans, M. Rosing, T. Tamura, and H.-D. Klenk. 1982. Post-translational glycosylation of coronavirus glycoprotein E1: inhibition by monensin. EMBO J. 1:1499-1504.

103. Niemann, H., R. Geyer, H.D. Klenk, D. Linder, S. Stirm, and M. Wirth. 1984. The carbohydrates of mouse hepatitis virus (MHV) A59: structures of the O-glycosidically linked oligosaccharides of glycoprotein E1. EMBO J. 3:665-670.

104. Okhuma, S., and B. Poole. 1978. Fluorescence probe measurement of the intralysosomal pH in living cells and the perturbation of pH by various agents. Proc. Natl. Acad. Sci. U.S.A. 75:3327-3331.

105. Oshiro, L.S., J.H. Schieble, and E.H. Lennette. 1971. Electron microscopic studies of coronavirus. J. Gen. Virol. 12:161-168.

106. Patterson, S., and M.R. Macnaughton. 1981. The distribution of human coronavirus strain 229E on the surface of human diploid cells. J. Gen. Virol. 53:267-273.

107. Patterson, S., and R.W. Bingham. 1976. Electron microscope observations on the entry of avian infectious bronchitis virus into susceptible cells. Arch. Virol. 53:267-273.

108. Pocock, D.H., and D.J. Garwes. 1977. The polypeptides of haemagglutinating encephalomyelitis virus and isolated subviral particles. J. Gen. Virol. 37:487-499.

109. Poste, G., and C.A. Pasternak. 1978. Virus-induced cell fusion, p. 305-357. In G. Poste and G.L. Nicholson (ed.), Cell Surface Reviews, vol. 4. Elsevier/North-Holland, Amsterdam.

110. Redmond, S.G. Peters, and C. Dickson. 1984. Mouse mammary tumor virus can mediate cell fusion at reduced pH. Virology 133:393-402.

111. Repp, R., T. Tamura, C.B. Boschek, H. Wege, R.T. Schwarz, and H. 1985. Niemann. The effects of processing inhibitors of N-linked oligosaccharides on the intracellular migration of glycoprotein E2 of mouse hepatitis virus and the maturation of coronavirus particles. J. Biol. Chem. 260:15873-15879.

112. Ricard, C.S., and L.S. Sturman. 1985. Isolation of the subunits of the coronavirus envelope glycoprotein E2 by hydroxyapatite high-performance liquid chromatography. J. Chromat. 326:191-197.

113. Rodriguez-Boulan, E. 1983. Membrane biogenesis, enveloped RNA viruses, and epithelial polarity. Mod. Cell Biol. 1:119-170.

114. Rottier, P.J.M., and J.K. Rose. 1987. Coronavirus E1 glycoprotein expressed from cloned cDNA localizes in the Golgi region. J. Virol. 61:2042-2045.

115. Rottier, P.J.M., M.C. Horzinek, and B.A.M. van der Zeijst. 1981.

Viral protein synthesis in mouse hepatitis virus strain A59-infected cells: effect of tunicamycin. J. Virol. 40:350-357.

116. Rottier, P., D. Brandenburg, J. Armstrong, B. van der Zeist, and G. Warren. 1984. Assembly in vitro of a spanning membrane protein of the endoplasmic reticulum: the E1 glycoprtein of coronavirus mouse hepatitis virus A59. Proc. Natl. Acad. Sci. U.S.A. 81:1421-1425.

117. Rottier, P., J. Armstrong, and D.I. Meyer. 1985. Signal recognition particle-dependent insertion of coronavirus E1, an intracellular membrane glycoprotein. J. Biol. Chem. 260:4648-4652.

118. Rottier, P.J.M., G.W. Welling, S. Welling-Wester, H.G.M. Niesters, J. A. Lenstra, and B.A.M. Van der Zeijst. 1986. Predicted membrane topology of the coronavirus protein E1. Biochemistry 25:1335-1339.

119. Scheid, A., and P.W. Choppin. 1974. Identification of biological activities of paramyxovirus glycoproteins. Activations of cell fusion, hemolysis and infectivity by proteolytic cleavage of an inactive precursor protein of Sendai virus. Virology 57:475-490.

120. Schochetman, G., R.H. Stevens, and R.W. Simpson. 1977. Presence of infectious polyadenylated RNA in the coronavirus avian infectious bronchitis virus. Virology 77:772-782.

121. Sharpee, R.L., C.A. Mebus, and E.P. Bass. 1976. Characterization of a calf diarrheal coronavirus. Am. J. Vet. Res. 37:1031-1041.

122. Siddell, S.G. 1983. Coronavirus JHM: coding assignments of subgenomic mRNAs. J. Gen. Virol. 64:113-125.

123. Siddell, S.G., A. Barthel, and V. ter Meulen. 1981. Coronavirus JHM: a virion-associated protein kinase. J. Gen. Virol. 52:235-243.

124. Siddell, S.G., R. Anderson, D. Cavanagh, K. Fujiwara, H.D. Klenk, M.R. Macnaughton, M. Pensaert, S.A. Stohlman, L. Sturman, and B.A.M. van der Zeijst. 1983. Coronaviridae. Intervirology 20:181-189.

125. Siddell, S.G., H. Wege, and V. ter Meulen. 1982. The structure and replication of coronaviruses. Curr. Top. Microbiol. Immunol. 99:131-163.

126. Simons, K., H. Garoff, and A. Helenius. 1982. How an animal virus gets into and out of its host cell. Sci. Am. 246:58-66.

126a. Sorensen, O., and S. Dales. 1984. In vivo and in vitro models of demyelinating disease: JHM virus in the rat central nervous

system localized by in situ cDNA hybridization and immunofluorescent microscopy. J. Virol. 56:434-438.

127. Spaan, W., H. Delius, M. Skinner, J. Armstrong, P. Rottier, S. Smeekens, B.A.M. van der Zeijst, and S.G. Siddell. 1983. Coronavirus mRNA synthesis involves fusion of non-contiguous sequences. EMBO J. 2:1839-1844.

128. Spaan, W.J., P.J.M. Rottier, M.C. Horzinek, and B.A.M. van der Zeijst. Isolation and identification of virus-specific mRNAs in cells infected with mouse hepatitis virus (MHV-A59). Virology, 108:424-434.

129. Spurr, A.R. 1969. A low viscosity embedding medium for electron microscopy. J. Ultras. Res. 26:31-43.

130. St. Cyr-Coats, K. 1987. Bovine enteropathogenic coronavirus: the effect of the host cell and trypsin modification on the virus structure, cytopathic expression and infectivity. Ph.D. dissertation, Louisiana State University, Baton Rouge, Louisiana.

131. Stair, E.L., M.B. Rhodes, R.G. White, and C.A. Mebus. 1972. Neonatal calf diarrhea: purification and electron microscopy of a coronavirus-like agent. Am. J. Vet. Res. 33:1147-1155.

132. Stern, D.F., and B.M. Sefton. 1982. Coronavirus proteins: Biogenesis of avian infectious bronchitis virus proteins. J. Virol. 44:794-803.

133. Stern, D.F., and S.I.T., Kennedy. 1980. Coronavirus multiplication strategy. I. Identification and characterization of virus specified RNA. J. Virol. 34:665-674.

134. Stohlman, S.A., J.O. Fleming, C.D. Patton, and M.M.C. Lai. 1983. Synthesis and subcellular localization of the murine coronavirus nucleocapsid protein. Virology 130:527-532.

135. Storz, J., R. Rott, and G. Kaluza. 1981. Enhancement of plaque formation and cell fusion of an enteropathogenic coronavirus by trypsin treatment. Infect. Immun. 31:1214-1222.

136. Sturman, L.S., and K.V. Holmes. 1982. The molecular biology of coronaviruses. Adv. Vir. Res. 28:35-112.

137. Sturman, L.S., and K.V. Holmes. 1985. Novel glycoproteins of coronaviruses. Tr. Biochem. Sci. 10:17-20.

138. Sturman, L.S., C.S. Ricard, and K.V. Holmes. 1985. Proteolytic cleavage of the E2 glycoprotein of murine coronavirus: Activation of cell-fusing activity of virions by trypsin and separation of two different 90K cleavage fragments. J. Virol. 56:904-911.

139. Sturman, L.S., K.V. Holmes, and J. Behnke. 1980. Isolation of coronavirus envelope glycoproteins and interaction with the viral nucleocapsid. J. Virol. 33:449-462.

140. Sugiyama K., and Y. Amano.1981. Morphological and biological properties of a new coronavirus associated with diarrhea in infant mice. Arch. Virol. 67:241-251.

141. Sugiyama, K. and R. Ishikawa. 1986. In vitro morphogenesis of the mouse coronavirus, DVIM. Sci. Rep. Hirosaki Univ. 33:15-18.

142. Sugiyama, K., and Y. Amano. 1980. Haemagglutination and structural polypeptides of a new coronavirus associated with diarrhoea in infant mice. Arch. Virol. 66:95-105.

143. Tartakaff, A.M. 1983. Perturbation of the structure and function of the Gogi complex by monovalent carboxylic ionophores. Meth. Enzymol. 98:47-59.

144. Tektoff, J., M. Dauvergne, M. Durafour, and J.P. Soulebot. 1983 Propagation of bovine coronavirus on VERO cell line: electron microscopic studies. Dev. Biol. Stand. 53:299-310.

145. Tompkins, W.A.F., A.M. Watrach, J.D. Schmale, R.M. Schultz, and J.A. Harris. 1974. Cultural and antigenic properties of newly established cell strains from adenocarcinomas of human colon and rectum. J. Natl. Cancer Inst. 52:101-106.

146. Tooze, J., S.A. Tooze. 1985. Infection of AtT20 murine pituitary tumour cells by mouse hepatitis virus strain A59: virus budding is restricted to the Golgi region. EMBO J. 37:203-212.

147. Tooze, J., S. Tooze, and G. Warren. 1984. Replication of coronavirus MHV-A59 in sac(-) cells: determination of the first site of budding of progeny virions. Eur. J. Cell Biol. 33:281-293.

148. Toth, T.E. 1982. Trypsin-enhanced replication of neonatal calf diarrhea coronavirus in bovine embryonic lung cells. Am. J. Vet. Res. 43-967-972.

149. Tycko, B., and F.R. Maxfield. 1982. Rapid acidification of endocytic vesicles containing a2-macroglobulin. Cell 28:643-651.

150. Tyrrell, D.A.J., J.D. Almeida, D.M. Berry, C.H. Cunningham, D. Hamre, M.S. Hofstad, L. Malluci, and K. McIntosh. 1968. Coronaviruses. Nature 220:650-659.

151. Tyrrell, D.A.J., J.D. Almeida, C.H. Cunningham, W.R. Dowdle, M.S. Hofstad, K. McIntosh, M. Tajima, L.Ya. Zakstelskaya, B.C. Easterday, A. Kapikian, and R.W. Bingham. 1975. Coronaviridae. Intervirology 5:76-82.

152. Vaananen, P., and L. Kaariainen. 1980. Fusion and haemolysis of erythrocytes caused by three togaviruses: Semliki, Sindbis, and Rubella. J. Gen. Virol. 46:467-475.

153. Van Dinter, S., and W.F. Flintoff. 1987. Rat glial C6 cells are defective in murine coronavirus internalization. J. Gen. Virol. 68:1677-1685.

154. Wege, H., M. Koga, R. Watanabe, K. Nagashima, and V. ter Meulen. 1983. Neurovirulence of murine coronavirus JHM termperature-sensitive mutants in rats. Infect. Immun. 39:1316-1324.

155. Wege, H., S. Siddell, and V. ter Meulen. 1982. The biology and pathogenesis of coronaviruses. Curr. Top. Microbiol. Immunol. 99:165-200.

156. Weiner, L.P. 1973. Pathogenesis of demyelination induced by a mouse hepatitis virus (JHM virus). Arch. Neurol. 28:298-303.

157. Weiss, S.R., and J.L. Leibowitz. 1983. Characterization of murine coronavirus RNA by hybridization with virus-specific cDNA probes. J. Gen. Virol. 64:127-133.

158. White, J., J. Kartenbeck, and A. Helenius. 1980. Fusion of Semliki forest virus with the plasma membrane can be induced by low pH J. Cell Biol. 87:264-272.

159. White, J., K. Matlin, and A. Helenius. 1981. Cell fusion by Semliki forest, influenza, and vesicular stomatitis viruses. J. Cell Biol. 89:674-679.

160. White, J., M. Kielian, and A. Helenius. 1983. Membrane fusion proteins of enveloped animal viruses. Rev. Biophys. 16:151-195.

161. Williams, J.R., and J. Storz. 1988. Trypsin-induced alterations of bovine coronavirus properties. In press.

162. Wilson, T.M.A. 1985. Nucleocapsid disassembly and early gene expression by positive-strand RNA viruses. J. Gen. Virol. 66:1201-1207.

CHAPTER IX: CURRICULUM VITAE

NAME: Harold Ross Payne

DATE AND PLACE OF BIRTH: October 23, 1952; Kingfisher, Oklahoma

PRESENT ADDRESS: 4250 Dodson Avenue
Baton Rouge, LA 70808

EDUCATION:	Dates	Degree	Major
Louisiana State University Baton Rouge, LA	1983-1988	Ph.D. Candidate	Veterinary Microbiology
Louisiana State University Baton Rouge, LA	1977-1982	M.S.	Microbiology
University of Oklahoma Norman, OK	1970-1975	B.S.	Microbiology
Kingfisher High School Kingfisher, OK	1966-1970		

EMPLOYMENT HISTORY:

1984-1988 Graduate Research Assistant. Department of Veterinary Microbiology and Parasitology, Louisiana State University. Baton Rouge, LA.

1980-1984 Research Associate. Department of Veterinary Anatomy and Fine Structure, Louisiana State University. Baton Rouge, LA.

1978-1979 Graduate Teaching Assistant. Department of Microbiology, Louisiana State University. Baton Rouge, LA.

1976-1977 Laboratory Technician. Department of Gynecology and Obstetrics, University of Oklahoma Health Sciences Center. Oklahoma City, OK.

AWARDS AND HONORS:

EMSA Presidential Graduate Student Award (1987)
LSEM Arceneaux Memorial Awards (1981, 1985)
Scientific Research Society of Sigma Xi (1987)
Travel Grant for the American Society for Virology 1986 Annual Meeting

MEETINGS ATTENDED:

South Central Branch of American Society for Microbiology (SCB/ASM; 1978-1987).
Louisiana Society for Electron Microscopy (LSEM; 1978-1987)
American Society for Virology (ASV; 1986)
American Society for Microbiology (ASM; 1978, 1982)
Electron Microscopy Society of America (EMSA; 1986, 1987)
Animal Disease Research Workers of the Southern States (ADRWSS; 1988)

PRESENTATIONS AT SCIENTIFIC MEETINGS:

Early events in bovine coronavirus infection of cultured cells. ADRWSS, April, 1988.

Expression of bovine coronavirus antigens at the plasma membrane in cultured cells. EMSA, August, 1987.

Inhibition of bovine coronavirus infection by chloroquine treatment. SCB/ASM, November, 1986.

Effects of chloroquine and ammonium chloride on the entry of bovine coronavirus into human rectal tumor cells. ASV, June, 1986.

Development of persistent infection of human rectal tumor (HRT) cells by bovine coronavirus. SCB/ASM, November, 1985.

Analysis by scanning electron microscopy of human rectal tumor cells resistant to lysis by bovine coronavirus. LSEM, May, 1985.

Organization of microtubule-like filaments in Azotobacter vinelandii. SCB/ASM, October, 1983.

Localization of terminal oxidase activity in Azotobacter with diaminobenzidine. ASM, March, 1982.

Cytochemical localization of cytochrome oxidase in Azotobacter vinelandii. SCB/ASM, October, 1981.

3,3'-Diaminobenzidine cytochemistry of Azotobacter vinelandii. LSEM, May, 1981.

PUBLICATIONS:

H.R. Payne and M.D. Socolofsky. 1984. Cytochemistry of cytochrome oxidase in the cytoplasmic and intracytoplasmic membranes of Azotobacter vinelandii. J. Bacteriol. 159:946-950.

H.R. Payne. 1987. Expression of bovine coronavirus antigens at the plasma membrane in cultured cells. In: G.W. Bailey, (ed.), Proceedings of the 45th Annual Meeting of the Electron Microscopy Society of America, p. 930-931, San Francisco Press, Inc., San Francisco, CA.

DOCTORAL EXAMINATION AND DISSERTATION REPORT

Candidate: Harold Ross Payne

Major Field: Veterinary Medical Sciences with option in Veterinary Microbiology and Parasitology

Title of Dissertation: Ultrastructural Studies of Cell Membrane-Associated Events in Early and Late Stages of Bovine Coronavirus Replication.

Approved:

Major Professor and Chairman

Dean of the Graduate School

EXAMINING COMMITTEE:

Date of Examination:

April 12, 1988